Heat Exchange Modeling for the Curing Process of Concrete

Route 30 Bridge over South Chuctanunda Creek,
Minaville, Town of Florida, Mongomery County New York

Final Report

December 1999

Gary S. Wojcik
And
David R. Fitzjarrald
Atmospheric Sciences Research Center
University of Albany, NY 12203

For
New York State Department of Transportation
1220Washington Avenue
Albany, New York 12232

In Cooperation with the Federal Highway Administration,
U.S. Department of Transportation
Washington, D.C.

DISCLAIMER

The Contents of this report reflect the views of the authors, who are responsible for the facts and the accuracy of the information presented herein. This document is disseminated under the sponsorship of the Department of Transportation, University Transportation Centers Program, in the interest of information exchange. The U.S. Government assumes no liability for the contents or use thereof.

TECHNICAL REPORT STANDARD TITLE PAGE

1. Report No.	2. Government Accession No.	3. Recipient's Catalog No.
497201311		

4. Title and Subtitle	5. Report Date
Heat Exchange Modeling for the Curing Process of Concrete	12/31/99
	6. Performing Organization Code

7. Author(s)	8. Performing Organization Report No.
Gary S. Wojcik and David R. Fitzjarrald, Ph.D.	

9. Performing Organization Name and Address	10. Work Unit No.
Atmospheric Sciences Research Center University at Albany, SUNY 251 Fuller Road Albany, NY 12203	11. Contract or Grant No. #497201311
	13. Type of Report and Period Covered Final Report 1/199 – 12/31/99
12. Sponsoring Agency Name and Address New York State Department of Transportation 1220 Washington Ave. Albany, NY 12232	14. Sponsoring Agency Code

15. Supplementary Notes

In cooperation with the Federal Highway Administration, U.S. Department of Transportation
Washington, D.C.

16. Abstract

This report describes the field campaign and subsequent data analysis for the June 1999 bridge project at the Route 30 bridge over the South Chuctanunda Creek in Montgomery County, NY. The two purposes of this work were 1.) to make more detailed measurements of the bridge environment than we have done in the past to better understand the energy budget of a curing concrete bridge and 2.) to provide atmospheric boundary conditions to a model of curing concrete. New measurements included direct sensible and latent heat fluxes above the bridge, sensible heat flux below the bridge, top surface concrete heat flux with heat flux plates, and air temperatures between the beams. We estimate that the amount of heat that was conducted toward the top surface during the peak internal temperatures was around 390 Wm-2. This heat was removed most efficiently by the runoff water heat flux (150 Wm-1 while the latent heat flux and net radiation each accounted for about 100 Wm-2. Heat loss below the bridge amounts to no more than 15% of the amount of heat removed at the top of the bridge. In computing the runoff water heat flux, we determined that the water that hits the top surface of the bridge does not reach the wet-bulb temperature of the air, as we have assumed in the past. Such an assumption can lead to errors in this budget term of up to 80Wm-2. About 95% of the water pumped onto the bridge runs off the bridge, with only 5% evaporating. From our energy budgets, we estimate that after 24 hours, this concrete bridge released about 210 kJ/kg-solid, which is in good agreement with our calorimetry estimates

17. Key Words	18. Distribution Statement
Bridges, Bridge Decks, Cement, PCC Concrete	None

19. Security Classif (of this report)	20. Security Classif. (of this page)	21. No of Pages	22. Price
Unclassified	Unclassified	54	

Form DOT F 1700.7 (8-69)

Table of Contents

Acknowledgments

The authors would like to thank the many people that made this research project possible. First we thank Ed Kulesa and the Tioga Construction crew for their assistance and patience throughout our field campaign. We also would like to thank the members of the Jungle Research Group for their help: Dr. Kathy Moore, Dwayne Spiess, Ralf Staebler, Ricardo Sakai, Otavio Acevedo, Jeff Freedman, and Behzad Abareshi. We thank Ralf Staebler again for providing the balloon measurements on the night of June 10. We are grateful to Dr. Gar Lala for his help and expertise in measuring the drop size of spray water from hoses similar to those used at the bridge. From NYSDOT, we thank Cheng Chou and Rick Morgan for their efforts to arrange this project and for their help in the field. Finally, we would like to thank the Research and Development Bureau of NYSDOT for supporting this work.

1. Introduction

The Jungle Research Group at ASRC made atmospheric and bridge environment measurements during and after the pouring of concrete at the Route 30 Bridge over the South Chuctanunda Creek in Florida, Montgomery County, NY from June 10-14, 1999. One purpose of this work was to make more detailed measurements than we have done in the past to better understand the energy budget of a curing bridge deck. Another reason for this work was to provide environmental boundary conditions for a model of curing concrete. We used our measurements and those made by the New York State Department of Transportation (DOT) to estimate the components of the surface energy balance at the top and the bottom of the bridge. Because the temperatures experienced by concrete during its curing stage can determine its strength and longevity, an understanding of the surface energy balance of the bridge under the current construction practices through observations and the modeling experiments could offer insight into optimal atmospheric conditions under which to initiate the pour.

Here we present a description of the Jungle Research Group's field campaign and subsequent data analysis. In section 2 of this report, we describe the measurements we made, the data delivered to DOT, and difficulties we encountered during the field operation. Section 3 contains a description of the weather during this period and the surface energy balance at the top and bottom of the bridge, including estimates of the amounts of chemical heat released by the concrete during this project. Finally, we present our conclusions and suggestions for future work in section 4.

2. Data

2.1 Instruments

We made measurements of the ambient environment both above and below the bridge and the top and bottom bridge surface environments. Figure 1 provides a top-down view of the location of many of the instruments we employed and Figures 2 and 3 provide schematics of instruments on our tower and instruments beneath the bridge, respectively.

At the top surface, four instrumented booms were extended from the east edge of the bridge to place instruments about 1 m above the bridge surface, 3 m from the east edge. Temperature probes known as thermistors were placed on the top surface of the bridge underneath the burlap to sample the surface temperatures of the concrete. A tipping bucket rain gauge and a wedge rain gauge were placed off the northeast corner of the bridge to record precipitation during the period. To determine the amount of water being pumped onto the bridge from the creek below, we used a flow meter which was located on the eastern side of the bridge.

Thermistors 1 through 6 were placed at varying distances from the east edge of the bridge and at two distances from the east edge (Figure 1) to provide a wide range of estimates of surface temperatures and to detect top surface temperature gradients. Specifically, Thermistors 1 and 4 were positioned above the east edge wooden form; Thermistors 2 and 5 sampled above the form; and Thermistors 3 and 6 were placed above the second support beam. Thermistor 7 was positioned to measure the temperature of the runoff water at the northeast corner of the bridge. We measured the temperature of the South Chuctanunda Creek with Thermistor 8. Thermistors 9 and 10 were taped to the bottom surface of the "stay-in-place" form on the underside of the bridge, at 6 and 12 m from the north edge, respectively (Figure 3).

Two REBS heat flux plates where positioned within the concrete, approximately 3.8 cm below the top surface of the concrete. These plates are indicated as F1 and F2 in Figure 1.

We measured incoming solar radiation on the top of the tower with an Eppley pyranometer, located approximately 2.5 meters above the top surface of the bridge (Figures 2 and 4). We also made horizontal wind speed observations at 2 m above the bridge surface with a Met One cup anemometer and a Gill propeller/vane anemometer, which is more sensitive to low wind speeds than is the Met One. The Gill also measured wind direction. For simplicity, we defined the direction North to South to point along the bridge from the north end to the south end. Therefore, for a wind direction of 360^{o}, the wind is blowing from the north end of the bridge straight toward the south end. Just below the wind observation level, we measured the air temperature and relative humidity with Campbell Scientific CS500 model probes.

Four booms were erected to support several instruments about 1 m about the bridge deck, 3 m from the east side of the deck (Figures 1 and 5). While the tower instruments provided the bulk atmospheric conditions in the area of the bridge, the instruments on the booms were intended to measure the atmospheric and bridge variables directly above the bridge. On Boom 1 (B1 in Figure 1), we mounted a Q7 net radiometer which viewed the bridge surface and the sky above and an Everest Interscience infrared thermometer which sampled the "skin" temperature of the bridge surface. The infrared thermometer was suspended approximately 7 cm above the surface and was shielded from the water spray by a large white funnel. Boom 2 contained Humitter temperature and relative humidity sensors at vertical two levels, 0.6 m (Humitter 1) and 1.4 m (Humitter 2). Boom 3 supported a Campbell Scientific krypton hygrometer which measured the specific humidity of the air and its fluctuations, while Boom 4 supported an ATI 3D sonic anemometer/thermometer which measured fluctuations in wind speed and direction and temperature.

The hygrometer and the sonic anemometer/thermometer provided proper data to compute directly sensible and latent heat fluxes above the bridge.

To measure the ambient conditions below the bridge, we installed a Q7 net radiometer, a Thornthwaite cup anemometer, and Campbell Scientific CS500 temperature and relative humidity probes approximately 6 m south from the north end bridge abutment, between the first two support beams from the east side (Figure 3). These instruments were approximately 0.9 m below the form and about 3 m above the creek. We sampled the air temperatures between the beams with thermocouples (TC1-TC5 in Figure 3) and we measured the temperatures of the east-most beam with thermocouples (TC6-TC9 in Figure 3). We also used an Everest Interscience infrared thermometer to measure the temperature of the bottom surface of the form. As mentioned earlier, thermistors 9 and 10 also sampled the temperature of the form. To measure high frequency wind and temperature fluctuations below the bridge, we mounted a Campbell Scientific 1D (vertical) anemometer and a Handar 2D sonic anemometer at the bottom of the support beams, as shown in Figure 3. These instruments were deployed to directly measure the sensible heat loss from between the beams.

We used instrumented balloons to measure profiles of temperature and humidity above the bridge and in the area surrounding the bridge. Figure 6 is a photograph of one of the balloons which we used. The data from these experiments have not been analyzed yet and so we do not discuss the balloon measurements further.

In short, many of the measurements we made for this field project were similar to those at previous bridge field projects. However, we made more detailed measurements directly over the bridge surface and below the bridge deck. New measurements included the high frequency temperature, humidity, and wind fluctuations, air temperatures between the support beams, and the

top surface concrete heat flux. Because of the inherent difficulties encountered in the June 1998 field project with measuring runoff water, we decided not to attempt continuous runoff rate measurements.

2.2 Data files

We provide to DOT three files containing the data collected during this field project on disk: 'BRID99datfil1', 'BRID99datfil2', and 'BRID99datfil3'. More specific information about the variables in these files is given in Tables I, II, and III, respectively. The variables for each file are written in vertical columns with each row giving the values at a given time. Each variable column is separated by blank spaces and missing values are given by 'NA'. The data were collected with 2 Campbell Scientific 23X dataloggers in the field in 5 minute averages from data sampled at 1 second intervals and are given as hourly averages in these files. The flow meter data are given as hourly totals.

We completed the preliminary placement of instruments by 8PM on Wednesday, June 9 (Julian Day 160). However, the first data point in the files is at 12AM on June 10, as final checks of the data system were not completed until 11PM on June 9. We collected data until 8AM on June 14 (Day 165). Note that our booms could not be extended out over the bridge until after the pour was complete and the burlap and hoses were placed which occurred at approximately 2PM on June 10 (Day 161). The data for the instruments on the booms are listed as 'NA' until that time. The thermistors on the top surface of the bridge were in place by 11 AM on June 10 when the burlap and hoses were set; the temperatures until that time are representative of air temperatures as the thermistors were hanging on the walkway railing on the east side of the deck.

Note that a sample of the concrete used for the deck was taken and its temperature moni-

tored with two thermocouples. These thermocouple temperatures are located in BRID99datfil1 are labeled as Concrete Temperature 1 and Concrete Temperature 2 in Table I.

We did encounter some difficulties in the field which led to some missing values and values which require additional explanation. First, we believe that the electronics cable for the Handar anemometer had a bad connection and so the Handar wind speed data (below the bridge) is not trustworthy. Fortunately, as a back-up, we also recorded the wind speed below the bridge with the Thornthwaite cup anemometer which provided reasonable wind speeds.

Because of some difficulties setting up our computer system in the DOT van, some of the data from the ATI sonic and the hygrometer were lost on the afternoon of June 10. In addition, a couple of hours of data is missing later in the period.

The heat flux plates used here were intended for use in a medium with a thermal conductivity approximately 1 W/m-K. Because the concrete used for this bridge has a conductivity of about 3.3 W/m-K (for Dolomite aggregate: Scanlon and McDonald, 1994), the heat flux plate measurements have been corrected as suggested by Philip (1961) and Fritschen and Gay (1979). The raw data was multiplied by 1.33 and 1.53, respectively, for plates 1 and 2. Because of the large corrections necessary for the plate data, the data must be viewed with some caution.

On the morning of June 11, the construction crew began work on the northern approach slab and on a sleeper slab at the south end of the bridge. In doing so, they removed Thermistor 7 from the runoff water stream, but it was replaced by ASRC personnel by 9AM. During this same time, a work bridge was pushed up against the net radiometer on Boom 1. The work bridge was moved away by 10AM and did not seem to affect the net radiation data. Also, the water pump was turned off during this period.

The Humitters on Boom 2 were placed in a short section of PVC pipe and aerated with a

small PC fan. Such hardware was used to make sure the sensors were making true readings of the air temperature and humidity and were not affected by direct sunlight or stagnant air. Apparently this setup was not enough to shield the sensor from the affects of the sun as afternoon temperatures recorded by the Humitters were about 1.2°C higher than other shielded temperature measurements with the CS500 probe on the tower. The Humitter humidity readings were about 3% lower than those from the CS500.

3. Results

3.1 Weather Overview

The period of observation was dominated by clear skies and light winds for the first 3 days and nights with partly cloudy skies occurring on the final day and night. No rain was measured during the period. The day of the pour (June 10) began with cloudy skies, but by the early afternoon, skies became clear, indicated in Figure 7 by a sharp increase in incoming solar radiation in the early afternoon.

Figure 8 shows the hourly averaged air temperatures and relative humidities during this period. With the clear days and nights, the air temperatures fluctuated from near 30°C during the day to near 9°C during the night. By the final 24-36 hours of observation, the partly cloudy conditions are evident in increased daytime humidities and nighttime temperatures.

Wind speeds above the bridge measured with the Gill anemometer were 1-1.5 m/s during the daytime periods and were near 0.7 m/s or lower during the night as is seen in Figure 9. Beneath the bridge, wind speeds were much lighter than those at the top of the bridge but were generally greater than 0.3 m/s. For much of the period, the wind at the top of the bridge blew

from the south end toward the north end, while the wind below the deck blew from the west to the east.

3.2 The Curing Slab

The pour began at 7AM on June 10 at the south end of the deck and the DOT thermocouples were covered with concrete by 9AM. The release of heat during the cure is evident both in the temperatures recorded by us and DOT. Figure 10 shows the hourly averaged concrete temperatures measured at various points in the concrete. DOT's temperature measurements between beams 2 and 3 from the east side at the top of the form and 189 mm and 108 mm up from the form and our measurements at the top surface and the bottom of the form show that the peak temperatures occurred near midnight on the night of June 10-11, about 15 hours after the pour was completed at this location. Peak internal temperatures reached 43°C between beams 2 and 3, while peak temperatures at the form bottom reached 40°C. The top surface temperatures show a double peak (29°C) from the afternoon of June 10 to the early morning hours of June 11. The first peak results from intense afternoon solar heating and is most pronounced in the upper layers of the concrete. The second peak at around midnight is produced by the heat released by the hydrating cementitious components in the concrete.

After midnight on the night of June 10-11, temperatures decreased as the internal heat source declined so that by June 12, the bridge became a more passive participant in its environment. At the top surface, we observed a more typical diurnal temperature variation with peak temperatures during the day and minimum temperatures during the night. Temperatures in the middle of the slab and at the top and bottom of the form showed more typical diurnal variations as well, except that the time of the maximum was increasingly lagged and the maximum magnitude

was damped from top to bottom as heat was being transferred from the top surface through the slab to the form. The rapid decrease in the surface and near surface level temperatures during late afternoons occurred when this area of the bridge deck was covered in shadows from trees as the sun began to set.

The hourly averaged net radiation (solar radiation + longwave radiation) measured above and below the bridge are shown in Figure 7. Note that positive values are net gains by the surface, whether it be top or bottom. At the top surface of the bridge, the net radiation exhibited a signature consistent of a passive surface throughout the period with a loss of radiation during the night and a net gain during the day. However, the net losses during the nights of June 10-11 (peaked at -93 Wm^{-2}) and June 11-12 (peaked at -80 Wm^{-2}) were considerably greater than other nights (peaked at -50 to -60 Wm^{-2}) which is indicative of the higher surface temperatures caused by the curing concrete during the first two nights.

The net radiation variation at the bottom of the bridge was much less pronounced than that at the top of the bridge, but still showed a peak magnitude (loss: 23 Wm^{-2}) during the night of June 10-11. During the time of the peak temperatures, the net radiation loss below the bridge was about 25% of the value at the top of the bridge.

3.3. Top Surface Energy Balance

3.3.1. Methodology

To compute the heat fluxes at the top surface, we use the bulk transfer approach in which the vertical flux, F, of a variable, X, is driven by the difference in X across an interface:

$$F_x = -V (X_{top} - X_{bottom}) \qquad (1)$$

where V is a transport velocity equal to C times U, where U is the mean wind speed and C is the

bulk transfer coefficient (Stull, 1988). C is dependent on the height above the surface at which measurements are made, the "roughness" of the surface, and atmospheric stability, as will be shown below. To determine C, we use Monin-Obukhov similarity theory and for conditions of free convection we determine the transport velocity by parameterizations given by Kondo and Ishida (1997).

Monin-Obukhov (M-O) similarity is an assumption that any dimensionless characteristic of turbulence depends only on friction velocity, u^*_0; the height above the ground, z; g/Θ_v, where Θ_v is the virtual potential temperature; and the surface heat flux, $\overline{w'\Theta v'}_0$. Consolidating these variables, M-O states that characteristics of turbulence depend on ζ=z/L, where L is the Monin-Obukhov length defined as:

$$L = -\frac{u^3_{*_o}}{k \cdot \frac{g}{\Theta_v} \cdot \overline{w'\Theta'_{v0}}} \tag{2}$$

M-O similarity is applicable in the constant flux layer (~lowest 10%) of the atmosphere, under conditions of horizontal homogeneity, when winds are non-zero, and when the flow is in equilibrium with the surface.

For the non-neutral case, the dimensionless wind profile can be written as:

$$\left(\frac{kz}{u^*_o}\right) \cdot \frac{\partial u}{\partial z} = \Phi_M(\zeta) \tag{3}$$

For Θ_v and q, the specific humidity, similar dimensionless profiles can be specified, respectively, as:

$$\left(\frac{kz}{\Theta_{v\,*}}\right) \cdot \frac{\partial \Theta_v}{\partial z} = \Phi_H(\zeta) \tag{4}$$

and

$$\left(\frac{kz}{q_*}\right) \cdot \frac{\partial q}{\partial z} = \Phi_W(\zeta) \tag{5}$$

where u_{*_0}, Θ_{*_0}, and q_{*_0} are scaling parameters (Garratt, 1992).

From these relationships, after integrating to determine functions for variable profiles, surface fluxes can be determined. For example, the heat flux, defined by $u_{*_0}\Theta_{*_0}$, is given by:

$$u_{*o}\Theta_{*o} = \frac{k^2}{\left[\ln\left(\frac{z}{z_0}\right) - \Psi_M(\zeta)\right]\left[\ln\left(\frac{z}{z_T}\right) - \Psi_H(\zeta)\right]} \cdot (u \cdot (\Theta_o - \Theta_v)) \qquad (6)$$

The first term on the right hand size is often called the "bulk transfer coefficient", C, as in equation 1. The value z_0 is the surface roughness parameter, which under neutral stability and horizontal homogeneity, can be viewed as the height at which the wind speed is zero. Under heterogeneous conditions, the flow may not be in equilibrium with the surface and so z_0 has no definite meaning and is a parameter chosen to describe the amount of drag exerted by the surface. The value z_T is the scaling length for temperature, which under neutral, horizontally homogeneous conditions, is the height above the surface at which the air temperature equals that of the surface.

Over immobile elements, z_0 is a function of surface geometry but not a function of wind speed or stability and does not change as long as the roughness elements do not change (Garratt, 1992). The z_0 for city centers may be 1 m, that for long grass may be 0.06 m, and that for snow may be 0.001 m (Stull, 1988).

As conditions become more unstable or as the roughness length increases, C increases as there is a greater transfer rate across an interface. The bulk transfer coefficients are most appropriate for large, homogeneous areas, which the bridges are not. In fact, z_0 for this bridge is not known and is probably variable across the bridge. Therefore, we compute C with two plausible roughness lengths of 0.005 m and 0.01 m and with stability considerations to bound C and therefore, our flux estimates.

M-O similarity theory must be modified under conditions in which wind speeds are light and large eddies are present. Under such conditions, the atmosphere is characterized by free convection where buoyancy fuels the atmospheric motions. In addition, the bulk transfer relations given above are no longer valid primarily because they are based on the surface shear stress produced by wind flowing over the surface. With no winds, the surface sheer stress does not exist.

Kondo and Ishida (1997) determined exchange speeds (which take the place of CU in the bulk relations) for free convection conditions over smooth or rough surfaces. They found that $CU=b(T_{sv}-T_{av})^{1/3}$, where b is .0011 for smooth surfaces and .0038 for rough surfaces and T_{sv} and T_{av} are the virtual temperatures of the surface and air, respectively. Free convective conditions were found during the night after the pour as the concrete surface temperature climbed to 29°C as the hydration reactions peaked. With wind speeds of about 0.5 m/s and a large air-surface temperature difference, buoyancy forces dominated atmospheric motions.

With these parameterizations of bulk transfer coefficients and exchange speeds, we estimate the energy budget at the top surface of the bridge. We employ the following sign convention: positive fluxes are upward. The energy balance we examine is:

$$-Q^*_A + Q_{GA} = Q_{HA} + Q_{EA} + Q_{RA} \qquad (7)$$

where $-Q^*_A + Q_{GA}$ is the available energy from net radiation, Q^*_A, and the concrete surface heat flux, Q_{GA}. The available energy must be balanced by the latent heat flux, Q_{EA}, the sensible heat flux, Q_{HA} and the heat removed by runoff water, Q_{RA}.

3.3.2 Latent and Sensible Heat Fluxes

For the bulk approach, expressions for Q_{EA} and Q_{HA} in units of Wm^{-2} are:

$$Q_{EA}=-\rho L_v C U (q_{air} - q_{sfc}) \quad (8)$$

and

$$Q_{HA}=-\rho c_p C U (T_{air} - T_{sfc}), \quad (9)$$

where q_{air} is the specific humidity (the mass of water vapor per unit mass of moist air) of air measured on the tower; q_{sfc} is the specific humidity of air at the surface, assumed to be the saturation value at the surface temperature; T_{air} is the temperature of air on the tower; T_{sfc} is the temperature of the surface; U is the mean wind speed measured with the ATI 3D sonic anemometer in m/s; ρ is the density of air; L_v is the latent heat of vaporization of water; and c_p is the specific heat of air.

We choose to compute Q_{EA} with Penman-Monteith considerations (Penman, 1948; Monteith, 1965). In this method, the specific humidity difference between the surface and the air in equation 8 is replaced by the linearization of the temperature versus saturation vapor concentration curve. Q_{EA} is then given by:

$$Q_{EA} = \rho L_v C U [s(T_{sfc} - T_{air}) + (q^*_{air} - q_{air})], \quad (10)$$

where s is the slope of the curve and q^*_{air} is the saturation specific humidity of air.

3.3.3. Runoff Water Heat Flux

Q_{RA} is computed with the change in temperature of the water sprayed onto the bridge and with the amount of water that runs off the bridge. We determine the amount of water running off the bridge by determining the amount of water that must evaporate to give Q_{EA} and subtracting that amount from the total amount pumped onto the bridge as measured by the flow meter.

In budget estimates for previous bridges, we assumed that the water temperature as it hits the surface is the wet-bulb temperature of air. A drop which has sufficient distance and time to

fall will reach the wet-bulb temperature of air (Kinzer and Gunn, 1951; Pruppacher and Klett, 1997). However, with experiments conducted here on the roof at CESTM, we have determined that in the short distance that the drops have to fall in the bridge setting, the drops may not reach the wet-bulb temperature.

When water is sprayed from the hoses and falls onto the bridge surface, its temperature changes due to the heat transfer from conduction from the air and evaporation. The relative rates of these two processes determine what the temperature of the drop will be when it hits the surface. The heat transfer rates depend on the drop size, the drop temperature, the air temperature, and the relative humidity of the air. For example, relatively speaking, a smaller drop at a higher temperature, in a higher air temperature environment will reach its wet-bulb temperature faster.

We measured the air temperature during the bridge field campaign and we measured the temperature of the water as it entered the pump (which we assume is the water temperature as it leaves the hose). To properly determine the temperature of the water as it hits the surface, we need to know the size of the drops. With the help of Dr. Gar Lala of ASRC, we measured the water drop sizes from hoses similar to those used at the bridge. Figure 11a shows the drop size distribution as number of drops per drop diameter per volume of air for 16 2 minute samples taken on September 2, 1999. For reference, a drop size prediction for a rainfall rate of 7 mm/hour, based on Marshall-Palmer's theory, is plotted. The most abundant drops were those less than 1 mm in diameter, although drops up to 1.5 mm in diameter show considerable density.

Since we are concerned with the volume of water coming from each drop size, we determine from the drop size distribution a rainfall rate contributed from each of several diameter bins. The results are shown in Figure 11b. The data suggest that about 90% of the water volume from the hose was from drops larger than 0.8 mm and about 60% was from drops larger than 1.5 mm.

With the air temperature, creek water temperature, the relative humidity, and a model described by Pruppacher and Klett (1997), we estimate the average temperature of water from a given bin assuming that the drop size is the mid-point of the bin; the drop fall speed is its terminal velocity if it is less than 0.8 mm in size or is less than its terminal velocity from drops larger than 0.8mm as given by Wang and Pruppacher (1977); and the drop travels a total distance of 4m (2m up and 2m down).

To determine the average temperature of the water as it hits the surface of the bridge, we weight the drop temperature of each bin by its fraction contribution to the total rainfall rate. The resulting water temperature is plotted in Figure 12 along with the wet-bulb, creek, and runoff water temperatures. Large errors would occur in the runoff water heat flux if we assume that the drops reach the wet-bulb temperature, especially at night when the air and creek temperatures are cooler. During the night, the temperature of the water as it hits the surface maybe as much as 7°C larger than the wet-bulb temperature. Given the amount of water pumped onto the bridge and this temperature difference, our estimates of Q_{RA}, if we assumed the drops reached their wet-bulb temperature, would be from 10 to 80 Wm^{-2} too high as compared to estimating Q_{RA} by assuming the drops slowly adjust in their environment as they fall. Therefore, in computing Q_{RA}, we assume that the water drops slowly adjust in their environment, as given by the Pruppacher and Klett (1997) model.

3.3.4. Net Radiation and Concrete Heat Flux

Q^*_A is measured. Q_{GA} is determined both as the residual of the other 4 terms and, as a reference, is determined directly by using the heat conduction equation:

$$Q_{GA} = -k\frac{dT}{dz} - \rho_c \cdot c_{pc} \cdot \Delta z \cdot \frac{dT}{dt} \qquad (11)$$

where Q_{GA} is in units of Wm^{-2}; k is the thermal conductivity (assumed to be 3.3 $Wm^{-1}K^{-1}$ for concrete); ρ_c and c_{pc} are the concrete density and specific heat capacities determined to be 2230 kg/m^3 and 1400 J/kg-K from a concrete sample taken during the pouring of the bridge; and dT/dz is the vertical temperature gradient within the slab between 162 mm and 216 mm up from the form as determined with the DOT slab temperature data. The second term on the right accounts for storage of heat in the concrete layer above the layer from which the first term on the right is determined.

3.3.5. Estimated Top Surface Fluxes

We compute the top surface energy budget with several assumptions about z_0 and exchange speeds. As mentioned earlier, we assume z_0 is 0.005 m (Scenario 1) and 0.01 m (Scenario 2) at all times. In addition, a third scenario begins with z_0 equal to 0.005. However, free convection exchange velocities as given by Kondo and Ishida (1997) are used for the first night when our measurements indicate free convection. The free convective conditions result from light winds and a surface-air temperature difference of more than 10°C as the hydrating cement led to surface temperatures of around 29°C and clear skies allowed the air to cool to as low as 10°C. During the daytime of June 11, the temperature difference between the surface and the air is greater than 10°C, as it is during the night of June 10. However, our measurements do not suggest free convection was occurring as wind speeds increased during the daytime up to about 1.5 m/s. Because of the large buoyancy forces generated by the surface-air temperature difference, it is

likely that the transfer rate on the afternoon of June 11 is somewhere between that under free convection and under fully forced convection with z0=0.005. Therefore, for the daytime hours of June 11, z_0 is set at 0.0025. Finally, our measurements of surface shear stress show a pronounced diurnal cycle (highest during the day) and we incorporate this fact into our budgets with a lower z0 during the night (z_0=0.003). All of these considerations are incorporated into Scenario 3, which represents our best estimate of the top surface energy budget.

Figure 13 shows the hourly averaged energy budget from Scenario 3. As discussed above, the hydrating cement began its main phase of heat generation during the evening of June 10 and peak concrete temperatures were found near midnight. At that time, Q_{GA} peaked at 390 Wm^{-2} and slowly decreased as the cure continued. Later in the period, Q_{GA} exhibited a diurnal variation which was typical of a passive bridge with a flux of heat into the surface during the day and a loss of heat from the surface at night. Q_{GA} during the final night of our observation period, when the heat generation by the hydrating cement was small, was a factor of 3 smaller than that during the first night when the hydrating cement released most of its heat.

Figure 14 shows the hourly averaged estimates of $-Q_{GA}$ for five different flux calculations and measurements. Scenario 4 is the estimate computed with the DOT thermocouple data and Scenario 5 are the corrected heat flux plate 1 values. Our estimates of the peak magnitude of Q_{GA} range from 300 to more than 600 Wm^{-2} with the aerodynamic methods on the night of June 10-11. The heat conduction method with the DOT thermocouple data gives a peak value of 393 Wm^{-2}, while Scenario 3, our best estimate, gives a peak of 387 Wm^{-2}. Later in the period, all estimates tend to converge.

Of all the scenarios presented in Figure 14, those from Scenario 3 best match the estimates

from the DOT data. During the night of June 10-11 when the surface temperatures are almost 30°C and wind speeds are very small, the use of free convection parameterizations clearly results in a better prediction than assuming z_0=0.005 or z_0=0.01.

We note that our measured $-Q_{GA}$ values from heat flux plate 1 (Scenario 5), with the proper corrections, are different from the DOT estimate by 25%, while showing a similar temporal variation. Because these plates are not intended for use in a medium with a high conductivity value as high as concrete, we view the measured values with caution.

The heat from Q_{GA} was removed from the top surface in $-Q^*_A$, Q_{EA}, Q_{HA}, and Q_{RA} which showed relative maxima during the night of June 10-11, in accord with Q_{GA} (Figure 13). Later in the period, these fluxes showed more typical diurnal variations with daytime maxima and nighttime minima. During the main heat generation period, the dominant heat removal mechanism was Q_{RA} which peaked at 150 Wm^{-2}, while Q_{EA} and $-Q^*_A$ had peak values around 95Wm^{-2} and Q_{HA} at 50Wm^{-2}. Note that had we assumed that the temperature of the water from the hoses was the wet-bulb temperature, Q_{RA} would have peaked at about 210 Wm^{-2} and $-Q_{GA}$ would have been -450 Wm^{-2}, or about 15% higher in magnitude than that from assuming the drops adjust slowly toward the wet-bulb temperature.

During the nights after June 10-11, $-Q^*_A$ is the dominant heat loss mechanism as the other terms approach zero. Without the internal heat source, the top surface and air temperatures decrease causing the surface-air temperature differences to be small. With a small buoyancy force and light winds, the transfer of heat from the surface is small.

The daytime top surface energy budget is dominated by $-Q^*_A$ as there was much incoming solar radiation under clear skies. Heat loss was mainly through evaporation which peaks at about

400 Wm^{-2}. Q_{HA} and Q_{RA} are less 100 Wm^{-2} when the bridge is more passive later in the period.

3.3.6 Measured Fluxes at the Top Surface

As mentioned earlier, we deployed instruments to measure the wind, temperature, and moisture fluctuations to provide a direct measurements of the latent and sensible heat fluxes above the bridge deck. With the fluctuations, the fluxes are given by:

$$Q_{EA} = \rho \cdot L_v \cdot \overline{w'q'} \tag{12}$$

$$Q_{HA} = \rho \cdot c_p \cdot (\overline{w'T'} + 0.84 \cdot \overline{T} \cdot \overline{w'q'}) \tag{13}$$

where w' is the fluctuation of the vertical wind component, q' is the humidity fluctuation, and T' is the temperature fluctuation. The second term in the parentheses on the right hand side of equation 13 results from the humidity variation of c_p, the specific heat capacity of air.

Figure 15 compares the measured latent and sensible heat fluxes to those estimated by free convection parameterizations and Scenario 3. After the first night, the latent heat flux observations compare very well with the free convection predictions (Figure 15a). However, the latent heat flux estimates from Scenario 3 are much larger than the observed or the free convection conditions. During the night of June 10-11, the observed latent heat flux is 50% of the predicted values.

During the nighttime, the observed sensible heat flux is similar to the free convection and Scenario 3 predictions. However, during the daytime, the observed sensible heat flux is much greater than both the free convection and Scenario 3 estimates.

It is not clear why our measured heat fluxes are so different from our Scenario 3 predic-

tions. Our flux estimates are based on Monin-Obukhov similarity theory, as discussed earlier. This theory is valid when the region consists of horizontally homogeneous surfaces, when winds are non-zero, and when the flow is in equilibrium with the surface. The bridge is a small feature in a complex area and so it is unlikely that the flow at every level has adjusted to the bridge surface. Therefore, our flux measurements are probably sampling fluxes from surfaces upwind of the bridge as air parcels floated passed our sensors and not fluxes applicable to the bridge surface. In other words, it is likely that an internal boundary layer developed over the bridge, particularly during the daytime when winds were stronger. This internal boundary layer was below the level of our instruments and so the observations are not in accord with the estimates.

During the nighttime, with large surface-air temperature differences and light winds, conditions were closer to free convection and so the internal boundary layer above the bridge was deeper. Because our instruments were in the internal boundary layer during the night, estimates and observations of the sensible and latent heat fluxes at night were closer than during the day.

3.3.7. Top Surface Water Budget

Figure 16 shows the budget of water pumped onto the bridge from the creek below. We metered the water from the pump and found that approximately 1000 gallons per hour were pumped. Because parts of hoses were not on the bridge surface, not all of this water landed on the top surface. We estimated at the time of the field operation that until the afternoon of June 11, 87% of the water pumped from the creek fell onto the bridge deck. After this time, some of the water was used to cure the sleeper slab at the south end of the bridge and so this percentage dropped to 75%. Therefore, for the duration of the period, between 800 and 900 gallons per hour were pumped onto the bridge deck. The water pump was turned off for a time on the morning of

June 11, which is evident in the drop in total pumped water and water reaching the deck in Figure 16.

Based on the evaporation estimate from Scenario 3, at most 40 gallons per hour evaporated during the afternoon, or about 5% of that which was pumped onto the bridge and the amount of runoff water was at least 95% of that pumped onto the bridge. Therefore, much less water could be used to cure the concrete, a fact that could be important in areas with limited water resources.

3.4. Bottom Surface Energy Balance

The energy budget below the bridge is given by:

$$-Q^*_B + Q_{GB} = Q_{HB} \qquad (14)$$

where Q^*_B is positive as a gain of radiation by the bottom of the bridge and negative as a loss and Q_{GB} and Q_{HB} are positive when energy is directed upward and negative when energy is directed downward. Note that Q_E and Q_R are not energy loss mechanisms below the bridge.

As seen in Figure 7, Q^*_B showed a peak loss of 25 Wm^{-2} during the night of peak internal temperatures, June 10-11. Over the entire period, Q^*_B changes sign from day to night but it was generally less than 20 Wm^{-2}.

Heat loss below the bridge as sensible heat occurred at two locations: the steel support beams and the form. Figure 17a shows the temperatures at various locations on the center support beam as measured by DOT with thermocouples. All levels on the beam experienced an increase in temperature around the time of peak concrete temperatures during the night of June 10-11 as the heat generated in the slab was conducted down the beam. The magnitude of the temperature rise was increasingly damped toward the lower levels of the beam as heat removal was enhanced

by higher wind speeds near the bottom of the beams.

Later in the period, the temperatures at all levels of the beam except the web joint and the top of the beam were very similar and showed a pronounced diurnal variation. The fins of the beams were heated by the air as it went through its diurnal temperature cycle. The fact that the temperatures on the fins were so uniform suggests that air was mixed up in between beams almost to the form rather effectively.

The top of beam and web joint temperatures reached their maximum and minimum several hours after the other points on the beams. The most likely reason for this is that the top of beam/ web joint were influenced more by the concrete slab than by the air below. Any heating or cooling that took place at these locations must have occurred as the concrete slab gained or lost heat from the top to bottom.

We estimate the amount of heat that was removed by the support beams by determining the heat flux into the top of the beam which is in contact with the concrete layer. Recall that the bridge support beams are in the shape of an "I" if a vertical cross section is taken. The horizontal cross-sectional area at the top of one beam is 0.42m x 27.4 m= 11.5 m^2. We estimate the flux across the beam/concrete interface by assuming a concrete thermal conductivity of 3.3 W/mK and considering the temperature difference across the bottom 27 mm of concrete. At peak heat generation times, the beams removed as much as 160 Wm^{-2}. Note that the beams are only in contact with about 20% of the bottom surface area of the concrete and so this heat removal was highly localized.

Figure 17b shows the air temperatures measured between the beams measured by the Jungle Research Group with thermocouples. The layer of air between the beams on the night of June 10-11 was highly stable with temperature differences of almost 15°C from near the form to the

bottom of the beams. On the afternoons of June 12 and June 13, the temperature gradients were erased as mechanical mixing occurs. However, the air temperatures at all layers between the beams increased coincidently while the temperature of the form increased at a different rate to a higher peak temperature. This suggests that the form's temperature was mainly dictated by heating or cooling from above, as was found for the top of the steel support beams. Therefore, heat loss or gain at the form by mechanical means is thought to be small. This fact explains why the temperatures at the top side of the form were higher than the concrete temperatures just above it during the peak heat generation period; if heat loss here were significant, the peak temperatures would be found at somewhat higher levels in the concrete.

Because the temperature of the form appears to be minimally influenced by mixing between the beams, conduction seems to be the likely mechanism of heat transfer here. The form is 0.47 cm thick and the air layer below it which we consider is 3.8 cm thick layer. The temperature difference we use is the difference between the top of the form and the air at 3.8 cm below the form. Assuming that half the form is insulated, we estimate the amount of heat that was conducted from the form to the air below was at most 2.5 Wm^{-2} during the peak heat generation period.

Combining the estimate from the beams and form with the net radiation, we compute the average heat loss below the bridge, as plotted in Figure 18a. Below the bridge, Q_{GB} peaked at -55 Wm^{-2} during the night of peak heat generation, which amounts to about 15% of the amount lost at the top of the bridge at this time. Most of this energy was from loss down the beams and the net radiation, while heat loss from the form was much smaller.

We consider our estimate of Q_{GB} below the bridge to be a maximum limit for 2 reasons. Our net radiometer was positioned between the beams, but at the level of the bottom of the beams.

Here, it measured radiation from the form and beams above it. Because the form is a shiny galvanized steel, its emissivity is low and so most of the net radiation value comes from the beams. However, in estimating the heat loss through the top of the beam, we have already accounted for the energy that was conducted down the beam and influenced the net radiation reading. Therefore, some of the energy is accounted for twice and so our estimate of Q_{GB} should be viewed as a maximum limit, particularly during the peak temperature period.

During its passive stage, the bottom of the bridge absorbed about 25 Wm^{-2} during the daytime and lost about 25 Wm^{-2} at night, again, mostly as a result of net radiation and the beams. These values are about 10% of the corresponding amounts at the top surface.

We measured heat loss from below the beams with a 1D Campbell sonic anemometer/thermometer mounted at the bottom of a beam (Figure 3). At this position, this instrument measured the heat as it left from between the beams and not necessarily the heat loss at the form or at different points along the beams as it was occurring.

To assess our measurements of heat loss from between the beams, we also make estimates of the heat loss from between the beams by using the bulk aerodynamic formula (equation 9). We assume that the mixing environment of the bridge is the same as would be encountered under the same stability conditions if the support beams protruded up from the ground.

The measured heat loss from between the beams and the aerodynamic estimate, assuming a roughness length of 0.35 m, are plotted in Figure 18b. (Note: from Lettau (1969), the roughness length of interest would be 0.25 m given the geometry and placement of the beams. However, a value of 0.35 m gives better agreement with the measured values later in the period). Heat was lost from this area from the time of peak heat generation until the morning of June 12. A small peak is evident during the time of peak curing temperatures as some heat was removed even

with the large stability and light winds. However, the maximum heat loss was recorded beginning at 8AM on June 11 as wind speeds began to increase and so increased the mechanical mixing between the beams. We argue that during the night of June 10-11, the heat removed from the slab, mostly by the beams, was dissipated to the air between the beams leading to the development of the stable layer of air. With light winds during this night, the mechanical mixing was small and only a small amount of heat was lost. By the morning of June 11, the wind speeds increased again and a large amount of heat was removed from between the beams. Similar enhanced mechanical mixing led to an upward heat flux on the afternoons of June 12 and June 13 as the warmer air surrounding the bridge was mixed between the beams.

We note that there is considerable discrepancy between the estimated and observed values, particularly when the air layer between the bridge is highly stable. The measurements suggest continual heat loss and so even under such highly stable conditions, warm parcels of air are dislodged with slight mechanical mixing, a process which is not well-described by our aerodynamic estimate. The stability of the layer between the beams approaches neutrality or even instability as on afternoons of June 12 and June 13, at which time our estimates and the observed are quite similar.

Our measured amount of heat loss from between the beams up to June 12 is about 50% of that estimated to be lost through the beams. Perhaps a portion of the heat was lost out the very bottom of the beams, below the level of measurement.

In general, our estimates of Q_{GB}, the estimate of heat loss from the beams, and the observed heat loss from between the beams suggest that heat loss from the bottom of the bridge deck was no more than about 15% of the loss from the top.

3.5. Chemical Heat Source

With our estimates of the top and bottom surface energy budgets and the DOT thermocouple data, we estimate the amount of heat generated by the hydrating cement, fly ash, and microsilica. We do this by integrating over the entire volume of the bridge deck. Aside from the two surface energy budgets, we must also consider the storage of energy within the concrete slab.

The internal volume budget equation is:

$$\Delta Q_S = -Q_{GA} + Q_{GB} + Q_I \tag{15}$$

where ΔQ_s is the storage term and Q_I is the internal chemical heat source.

The storage term is computed from the DOT slab temperature data taken above the form:

$$\Delta Q_s = \rho_c \cdot c_{pc} \cdot \Delta z \cdot \sum_{z=1}^{9} \frac{\Delta \bar{T}(z)}{\Delta t} \tag{16}$$

where the change in the average temperature of each of 9 layers over each hour is multiplied by the thickness of the layer and summed over the nine layers. A positive value indicates a net storage of heat and a negative value indicates a net loss of heat.

By integrating over the entire volume of the bridge, it is possible to determine Q_I from the relation:

$$Q_I = Q_{HA} + Q_{EA} + Q_{RA} + Q^*_A - Q_{HB} - Q^*_B + \Delta Q_s \tag{17}$$

Figure 19 shows the chemical heat evolution rate for Scenarios 1-4 and for a calorimetry experiment performed on the Class HP concrete mix sample from the June 1998 bridge. For Scenario 4, the individual budget terms in equation 17 are replaced with the Q_{GA} and Q_{GB}. We assume that Scenario 4 provides the best description of the actual heat evolution from the concrete at this bridge and shows that shortly after noon on June 10, the concrete began to generate heat. This heat generation rate reached a peak of 7 J/s-kg-solid at around midnight and from there the rate

quickly decreased to near zero so that after about 24 hours, we detected very little heat generation. The Scenario 3 rate follows the Scenario 4 rate very closely, although the Scenario 3 peak is somewhat higher. Scenarios 1 and 2 in comparison to Scenario 4 are considerably different and show some obviously inaccurate peaks.

The Scenario 4 rate follows the calorimetry rate very closely, although the peak heat rate from Scenario 4 is greater than that from the calorimetry. We also note that after about 18 hours, Scenario 4 more rapidly drops to zero than does the calorimetry rate. One reason for these differences could be that the cement used in the June 1998 bridge was considerably different than that in the June 1999 bridge. We will investigate this further in laboratory studies. Another possible reason for the increased peak heat generation rate is that some of the concrete for the June 1999 bridge reached peak temperatures which were about 5°C higher than experienced by the calorimetry sample. A higher temperature produces a more rapid heat generation rate.

The heat generation rates of the concrete for each scenario are integrated over the first 24 hours and over the first 72 hours and the results are shown in the legend of Figure 19. The amount of heat generated over the first 24 hours as suggested by Scenarios 3 and 4 ranges from 203 to 218 kJ/kg-solid, which is in agreement with the calorimetry. Over the first 72 hours, the totals are slightly different with Scenarios 3 and 4 being about 4% less than the calorimetry total. As we move past the peak heat generation period of the first 24 hours, it becomes increasingly more difficult for our budget estimates to be able to detect the tiny amounts of heat that were generated at these times. Therefore, values for 72 hours from our budget estimates are uncertain. The results from Scenarios 1 and 2 clearly show that inaccuracies may be introduced into the chemical heat source by incorrect assumptions about the amount of surface stress experienced by the bridge's top surface.

4. Conclusions

We have successfully measured the important atmosphere and bridge environment variables necessary to estimate energy balances of the curing bridge deck on Route 30 over the South Chuctanunda Creek. Differences in our measurements for this project in comparison to those in past years included direct flux measurements, the concrete heat flux measured with heat flux plates, air temperatures between the beams, and no continuous runoff water samples.

We estimate that the concrete heat flux at the top surface of the bridge at peak internal temperatures was about 385 Wm^{-2}, with a range between 300 Wm^{-2} and 600 Wm^{-2}, for a variety of assumptions. Estimates based on the DOT thermocouple data suggest approximately 390 Wm^{-2}. This heat was most efficiently removed from the top surface by the runoff water heat flux (150 Wm^{-2} at its peak), but the net radiation and latent heat fluxes also contributed significant amounts (100 Wm^{-2}). The sensible heat flux accounted for less than 50Wm^{-2}.

For the bottom of the bridge, we estimate that the total heat loss during the peak internal temperatures was no more than 55 Wm^{-2}. Most of this flux was from the net radiation and the beams. Heat loss from the beams was locally 160 Wm^{-2}, but when scaled to the entire area of the bridge contributed 32 Wm^{-2}.

Later in the observation period, when the heat generation in the slab was small, the daytime heat fluxes were dominated by the latent heat flux and the net radiation and $-Q_{GA}$ reached as high as 320 Wm^{-2}. At night, Q_{GA} reached a peak of about 120 Wm^{-2}, or about 33% of the amount during the peak heat generation period.

Our measured sensible and latent heat fluxes were quite different from our estimated

fluxes. The most likely reason for this is that our instruments sampled air which was above an internal boundary layer which developed over the bridge. We will continue to work on this issue.

In estimating the runoff water heat flux, we had previously assumed that the temperature of the drops as they hit the bridge surface was the wet-bulb temperature of the air. Experiments done on the roof at ASRC and a model of drop temperatures suggests that most of the drops do not spend sufficient time in the air to reach the wet-bulb temperature. We estimate that for this project the water drops were actually as much as 7°C warmer than the wet-bulb temperature with the largest differences occurring at night. The night time errors in Q_{RA} could be as high as 80 Wm^{-2} if this information is not considered.

As we found with the June 1998 bridge, most of the water pumped onto the bridge runs off. We estimate that at most 5% of the water evaporates, suggesting that the amount of water pumped onto the bridge could be reduced significantly, if water resources are limited.

From the energy budgets, we estimate the chemical heat source for this bridge to be about 210 kJ/kg-solid after 24 hours; our estimate of this value from calorimetry of the cementitious components from the June 1998 bridge suggest about 200 kJ/kg-solid, as well. Our estimates over a 72 hour period are about 4% lower than the calorimetry estimate (230 vs. 240 kJ/kg-solid). We recognize that cementitious components on the 1998 bridge may be different than those used in the most recent bridge. However, we feel that the close agreement of our estimated chemical heat source and the calorimetry is encouraging. We will conduct more calorimetry on the cementitious samples of the most recent bridge as soon as they are received.

As mentioned earlier, work will continue with the flux data. In addition, we will begin to examine the balloon temperature and humidity profiles collected during the night of June 10-11. Aside from planned calorimetry experiments, we will begin work on determining a chemical reac-

tion mechanism of hydrating cementitious compounds for use in models of curing concrete. These models will be used to understand the effects of changing atmospheric conditions on the thermal structure of the curing concrete slab.

5. References

Fritschen, L. J. and L. W. Gay, 1979: Environmental Instrumentation, Springer-Verlag, New York.

Garratt, J. R., 1992: T*he atmospheric boundary layer.* Cambridge University Press, 316pp.

Lettau, H., 1969: Note on aerodynamic roughness-parameter estimation on the basis of roughness-element description, *J. Appl. Meteor.*, **8**, 828-832.

Monteith, J. L., 1965: Evaporation and advection. *Symp. Soc. Exp. Biol.*, **19**, 205-234.

Penman, H. L., 1948: Natural evaporation from open water, bare soil, and grass. *Proc. Roy. Soc. London*, **A193**, 120-195.

Philip, J. R., 1961: The theory of heat flux meters. *J. Geophys. Res.*, **66**, 571-579.

Pruppacher, H. R. and J. D. Klett, 1997: *Microphysics of clouds and precipitation,* Klumer Academic Publishers, Boston, 954pp.

Scanlon, J. M. and J. E. McDonald, 1994: Thermal properties: in *Significance of tests and properties of concrete and concrete-making materials*, P. Klieger and J. F. Lamond, eds., American Society for Testing and Materials.

Stull, R. B., 1988: *An introduction to boundary layer meteorology.* Kluwer Academic Publishers, Boston, 666pp.

Wang, P. K. and H. R. Pruppacher, 1977: Acceleration to terminal velocity of cloud and raindrops, *J. Meteor.*, **16**, 275-280.

Table I. Variables in datafile 'BRID99datfil1'. See Section 2 and Figures 1-5 for details.

Column Number	Variable Name	Units	Begin Time	End Time
1	Day	Julian Day	0000, Day 161	800, Day 165
2	Time	Local Time	0000, Day 161	800,Day 165
3	Incoming Shortwave Radiation from Tower (Eppley Pyranometer)	Wm^{-2}	0000, Day 161	800, Day 165
4	Net Radiation Above Bridge (Q7)	Wm^{-2}	1400, Day 161	800, Day 165
5	Net Radiation Below Bridge (Q7)	Wm^{-2}	0000, Day 161	800, Day 165
6	Heat Flux Plate 1	Wm^{-2}	0000, Day 161	800, Day 165
7	Heat Flux Plate 2	Wm^{-2}	0000, Day 161	800, Day 165
8	Infrared Thermometer at Top of Bridge	^oC	1600, Day 161	800, Day 165
9	Infrared Thermometer at Bottom of Bridge	^oC	0000, Day 161	800, Day 165
10	Humitter Air Temperature 1 (Boom 2)	^oC	0000, Day 161	800, Day 165
11	Humitter Air Temperature 2 (Boom 2)	^oC	0000, Day 161	800, Day 165
12	Humitter Relative Humidity 1 (Boom 2)	%	0000, Day 161	800, Day 165
13	Humitter Relative Humidity 2 (Boom 2)	%	0000, Day 161	800, Day 165
14	Datalogger Temperature	^oC	0000, Day 161	800, Day 165
15	Concrete Sample Temperature 1	^oC	800, Day 161	800, Day 165

Table I, continued

Column Number	Variable Name	Units	Begin Time	End Time
16	Concrete Sample Temperature 2	^{o}C	800, Day 161	800, Day 165
17	Gill Wind Speed (tower)	m/s	0000, Day 161	800, Day 165
18	Gill Wind Direction (tower)	o	0000, Day 161	800, Day 165
19	Gill Wind Direction Standard Deviation (tower)	o	0000, Day 161	800, Day 165
20	Flowmeter	gallons per hour	700, Day 161	800, Day 165
21-35	Standard Deviations of Variables 3 through 17	Depends on Variable	Depends on Variable	800, Day 165

Table II. Variables in datafile 'BRID99datfil2'. See Section 2 and Figure 1,3, and 5 for details.

Column Number	Variable Name	Units	Begin Time	End Time
1	Day	Julian Day	0000, Day 161	800, Day 165
2	Time	Local Time	0000, Day 161	800,Day 165
3	Specific Humidity (Krypton Hygrometer--Boom 3)	$g\ m^{-3}$	1400, Day 161	800, Day 165
4	ATI 3D Sonic Horizontal Wind Speed (Boom 4)	m/s	1400, Day 161	800, Day 165
5	ATI 3D Sonic Horizontal Wind Speed (Boom 4)	m/s	1400, Day 161	800, Day 165
6	Handar 2D Sonic Horizontal Wind Speed (below bridge)	m/s	1200, Day 161	800, Day 165
7	Handar 2D Sonic Wind Direction (below bridge)	o	1200, Day 161	800, Day 165
8	Handar 2D Sonic Wind Direction Standard Deviation (below bridge)	o	1200, Day 161	800, Day 165
9-11	Standard Deviation of Variables 3-5	Depends on Variable	Depends on Variable	800, Day 165

Table III. Variables in datafile 'BRID99datfil3'. See Section 2 and Figures 1-5 for details.

Column Number	Variable Name	Units	Begin Time	End Time
1	Day	Julian Day	0000, Day 161	800, Day 165
2	Time	Local Time	0000, Day 161	800,Day 165
3	Datalogger Temperature	^{o}C	0000, Day 161	800, Day 165
4	Thermocouple 1	^{o}C	0000, Day 161	800, Day 165
5	Thermocouple 2	^{o}C	0000, Day 161	800, Day 165
6	Thermocouple 3	^{o}C	0000, Day 161	800, Day 165
7	Thermocouple 4	^{o}C	0000, Day 161	800, Day 165
8	Thermocouple 5	^{o}C	0000, Day 161	800, Day 165
9	Thermocouple 6	^{o}C	0000, Day 161	800, Day 165
10	Thermocouple 7	^{o}C	0000, Day 161	800, Day 165
11	Thermocouple 8	^{o}C	0000, Day 161	800, Day 165
12	Thermocouple 9	^{o}C	0000, Day 161	800, Day 165
13	Thermistor 1	^{o}C	0000, Day 161	800, Day 165
14	Thermistor 2	^{o}C	0000, Day 161	800, Day 165
15	Thermistor 3	^{o}C	0000, Day 161	800, Day 165
16	Thermistor 4	^{o}C	0000, Day 161	800, Day 165

Table III, continued

Column Number	Variable Name	Units	Begin Time	End Time
17	Thermistor 5	°C	0000, Day 161	800, Day 165
18	Thermistor 6	°C	0000, Day 161	800, Day 165
19	Thermistor 7	°C	0000, Day 161	800, Day 165
20	Thermistor 8	°C	0000, Day 161	800, Day 165
21	Thermistor 9	°C	0000, Day 161	800, Day 165
22	Thermistor 10	°C	0000, Day 161	800, Day 165
23	CS500 Temperature 1 (on tower)	°C	0000, Day 161	800, Day 165
24	CS500 Temperature 2 (below bridge)	°C	0000, Day 161	800, Day 165
25	CS500 Relative Humidity 1 (on tower)	%	0000, Day 161	800, Day 165
26	CS500 Relative Humidity 2 (below bridge)	%	0000, Day 161	800, Day 165
27	Thornthwaite Cup Anemometer Wind Speed (below bridge)	m/s	0000, Day 161	800, Day 165
28	METOne Cup Anemometer Wind Speed (tower)	m/s	0000, Day 161	800, Day 165
29-54	Standard Deviations of Variables 3-28	Depends on Variable	Depends on Variable	800, Day 165
55	Tipping Bucket Rain Gauge	mm/hour	0000, Day 161	800, Day 165

Location of Instruments at the Top and Sides of the Bridge

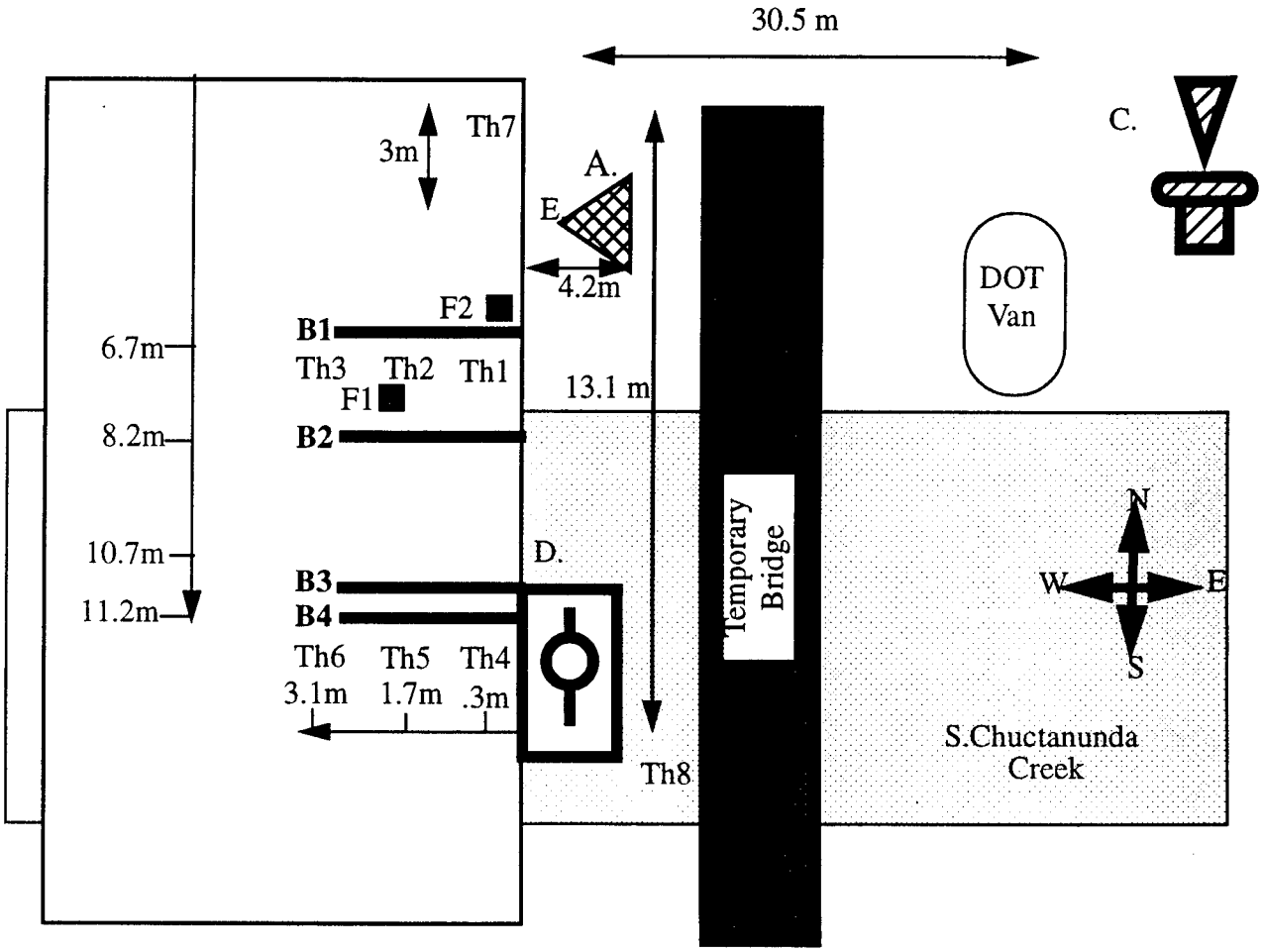

Instruments on Booms:

B1: Net Radiometer/IR Thermometer
B2: 2 Humitters (Temp/RH)
B3: Krypton Hygrometer
B4: 3-D Sonic Anemometer

Key:
A: Instrumented Tower
B1-B4: Instrumented Booms
C: Rain Gauges
D. Flow Meter
E. Dataloggers
F1-F2: Heat Flux Plates
Th1-Th8: Thermistors (1-8)

Figure 1. The locations of instruments and other hardware on the top and sides of the bridge.

Instruments on Tower

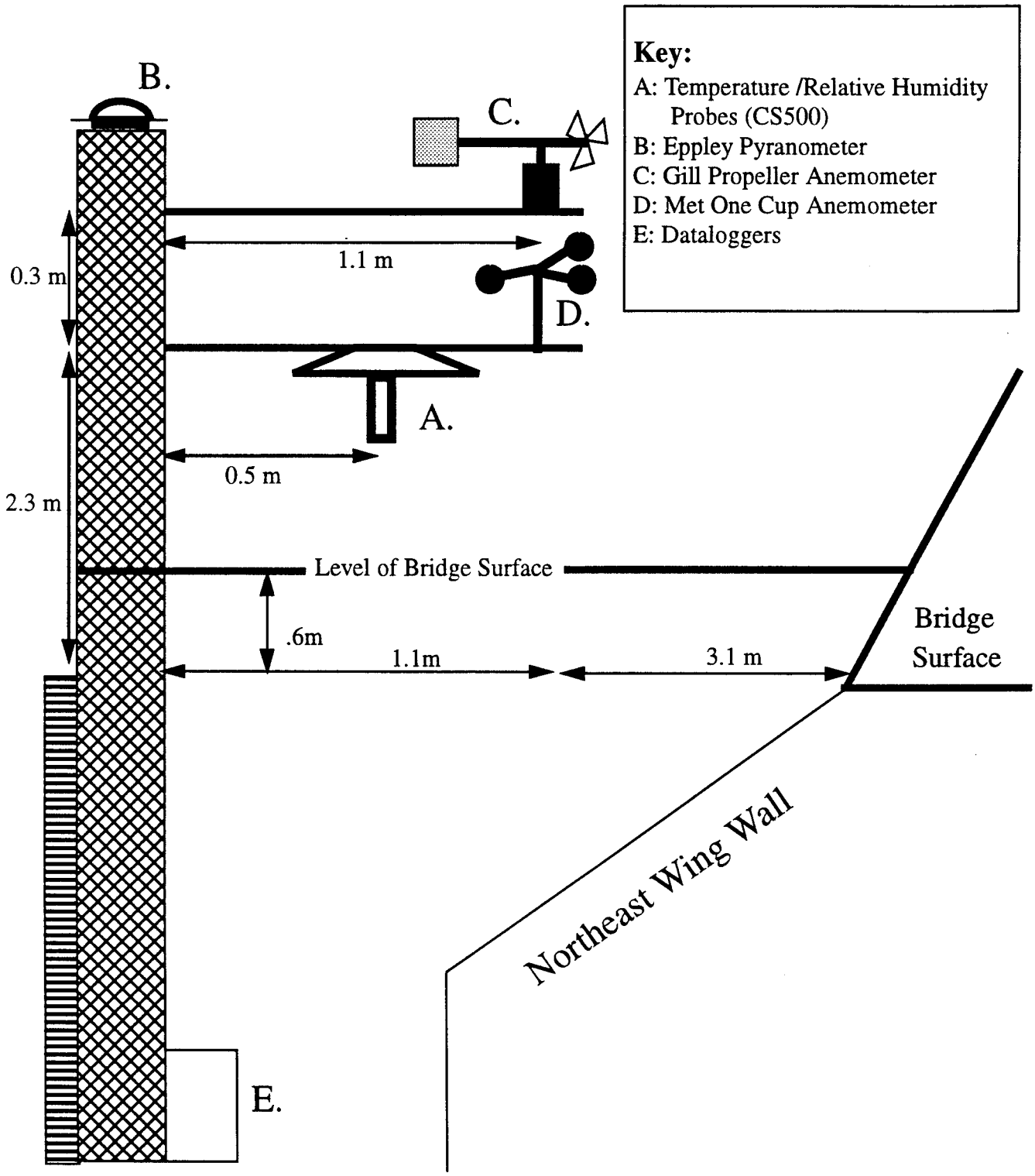

Figure 2. Schematic of the instruments on the tower looking south from the northeast corner of the bridge.

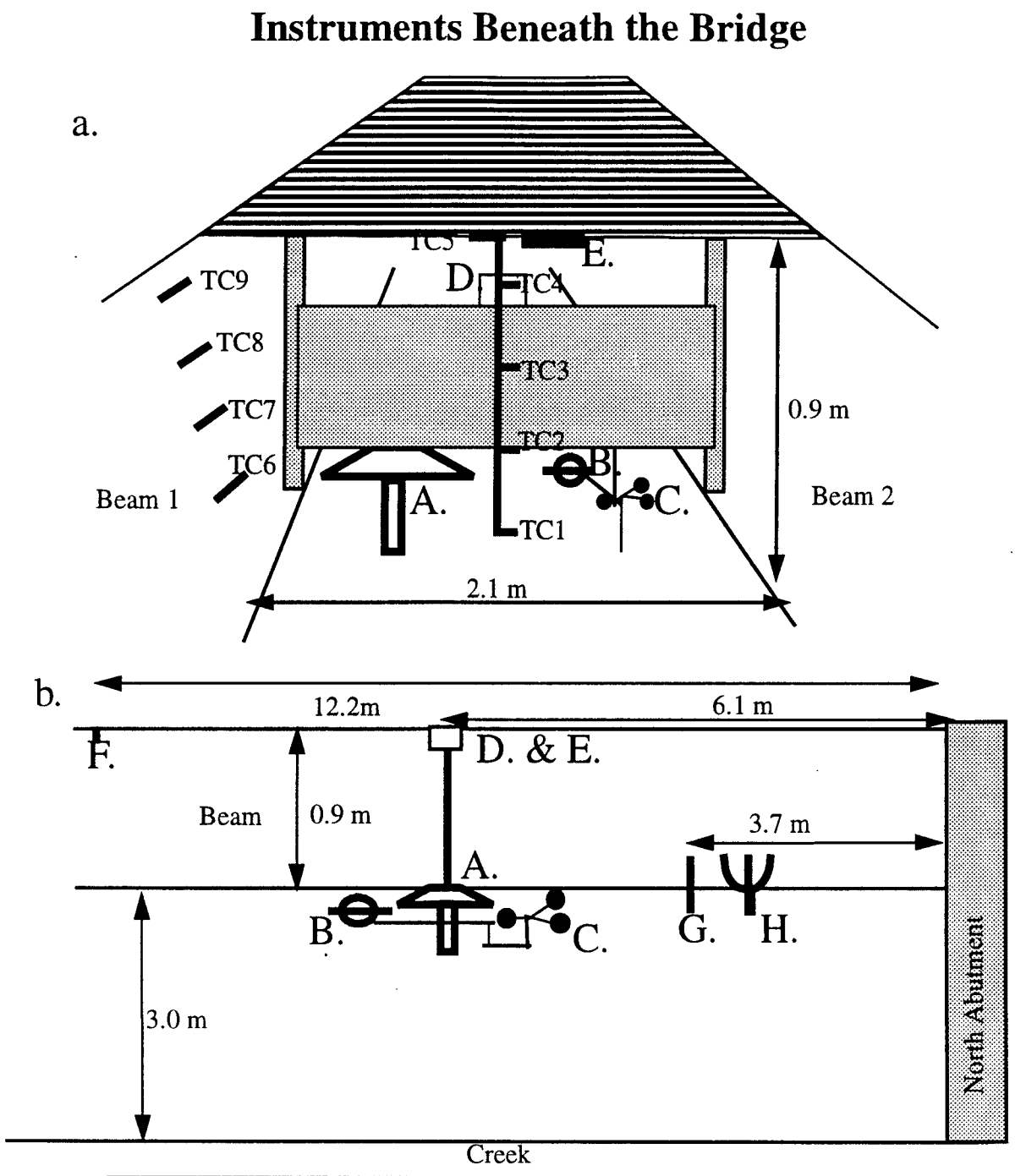

Figure 3. Schematic picture of instruments mounted beneath the bridge between Beams 1 and 2 from the east edge. **a**. Looking North to South. **b**. Side view, looking East to West. Note that TC1-TC5 measured air temperatures while TC6-TC9 measured the beam temperatures..

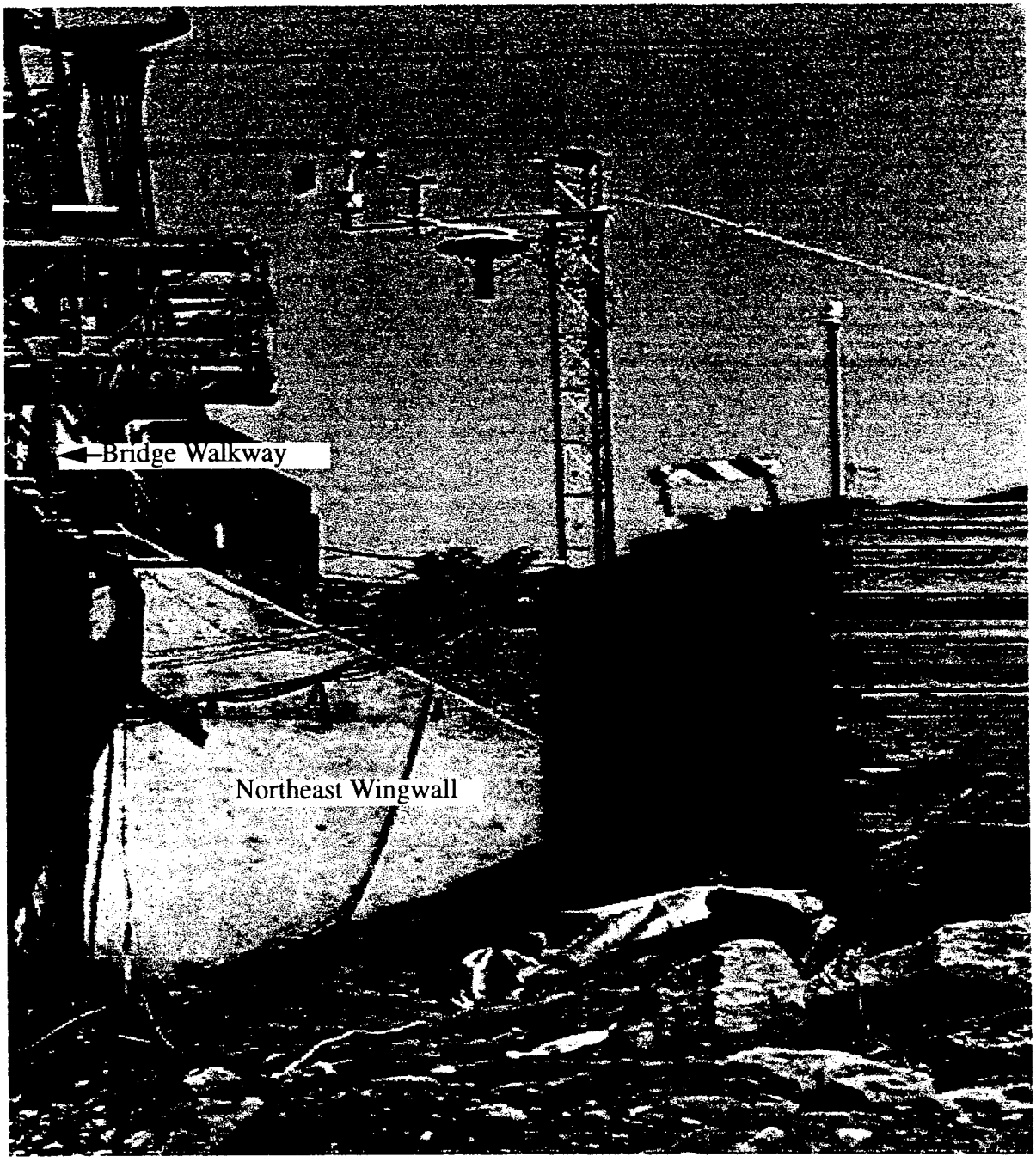

Figure 4. A photograph of the ASRC tower looking from South to North. The bridge deck is on the left side of the picture.

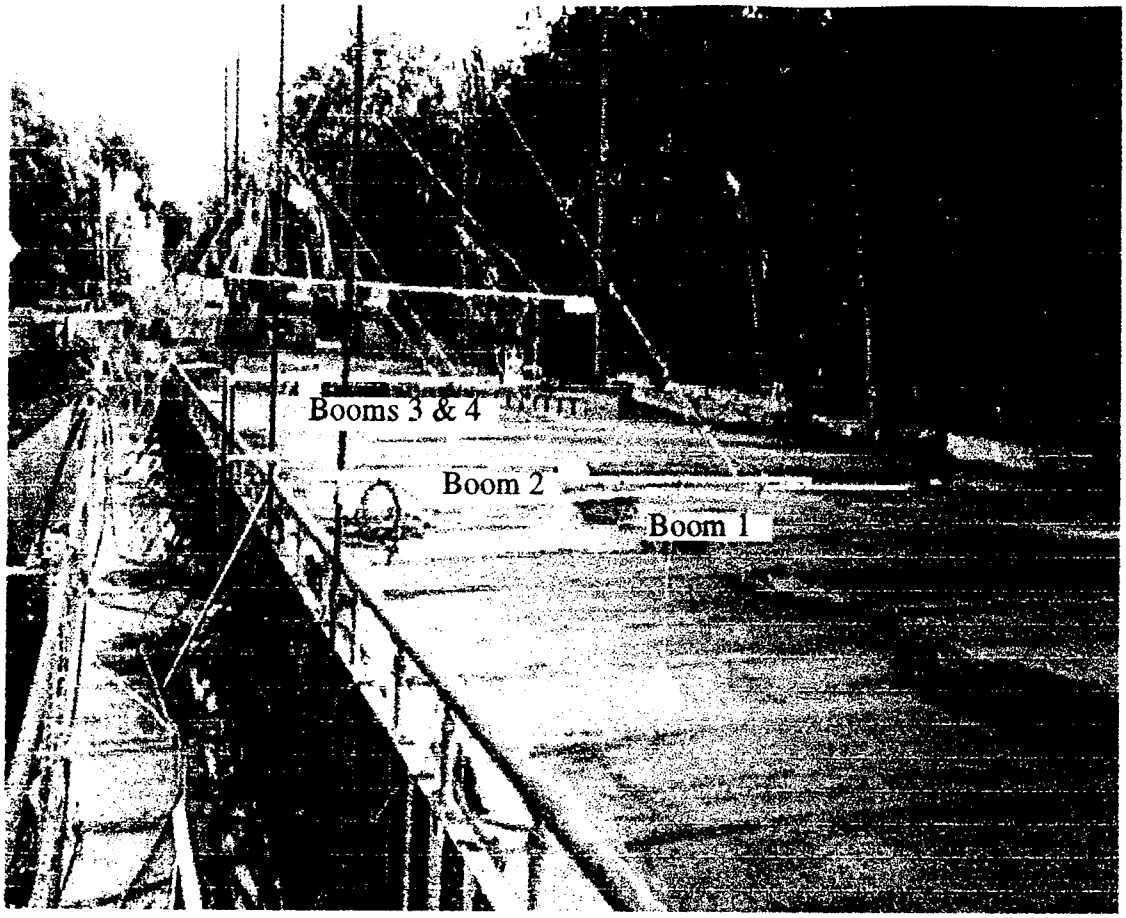

Figure 5. A photograph of the instrumented booms deployed over the bridge deck looking from North to South.

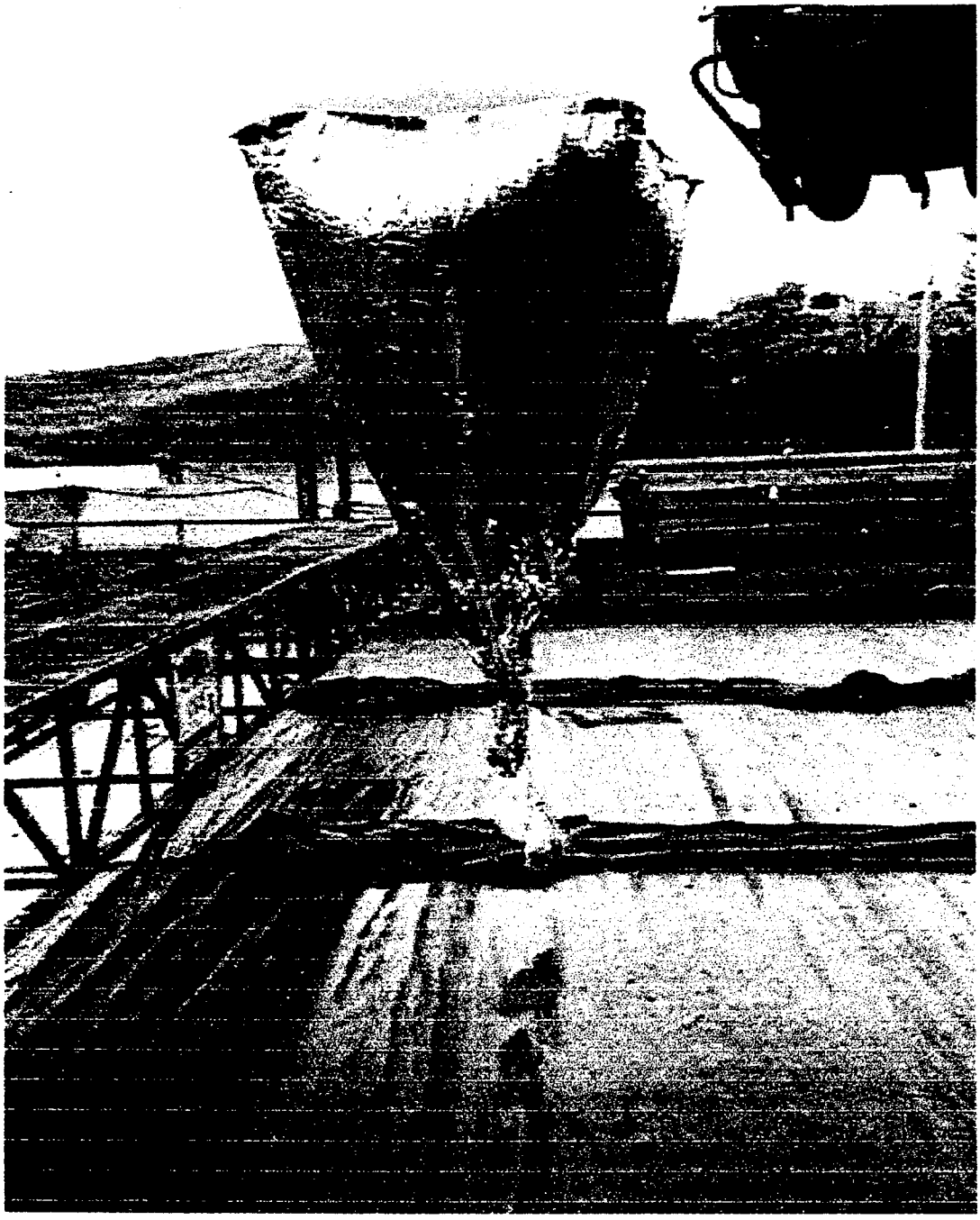

Figure 6. A photograph of one of the balloons used during the field campaign. This balloon was used to measure temperature and humidity profiles horizontally across the bridge at several different heights.

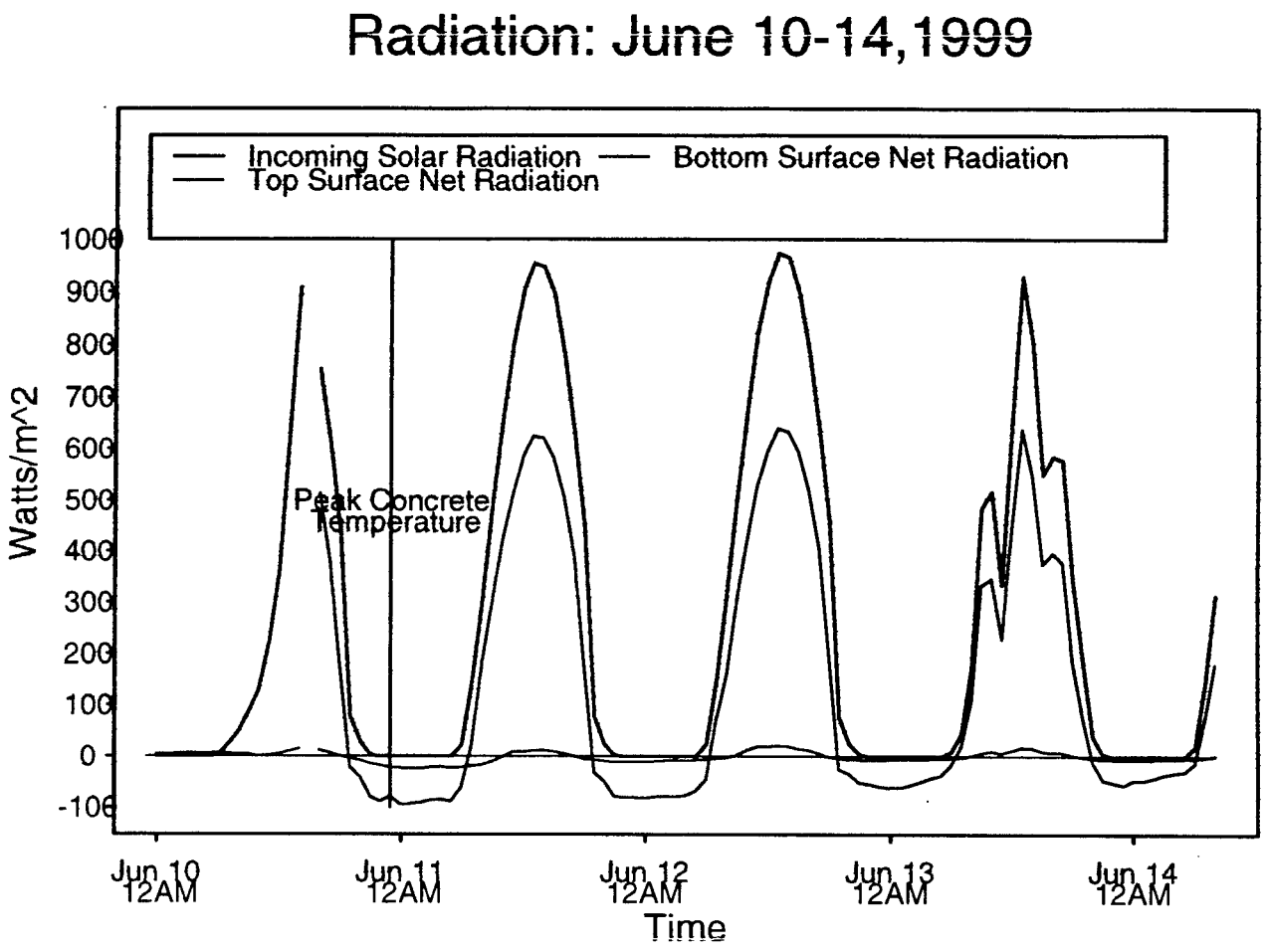

Figure 7. Hourly averaged measured radiation variables. For these variables, a positive value indicates a gain of energy by the surface and a negative value indicates a loss of energy from the surface.

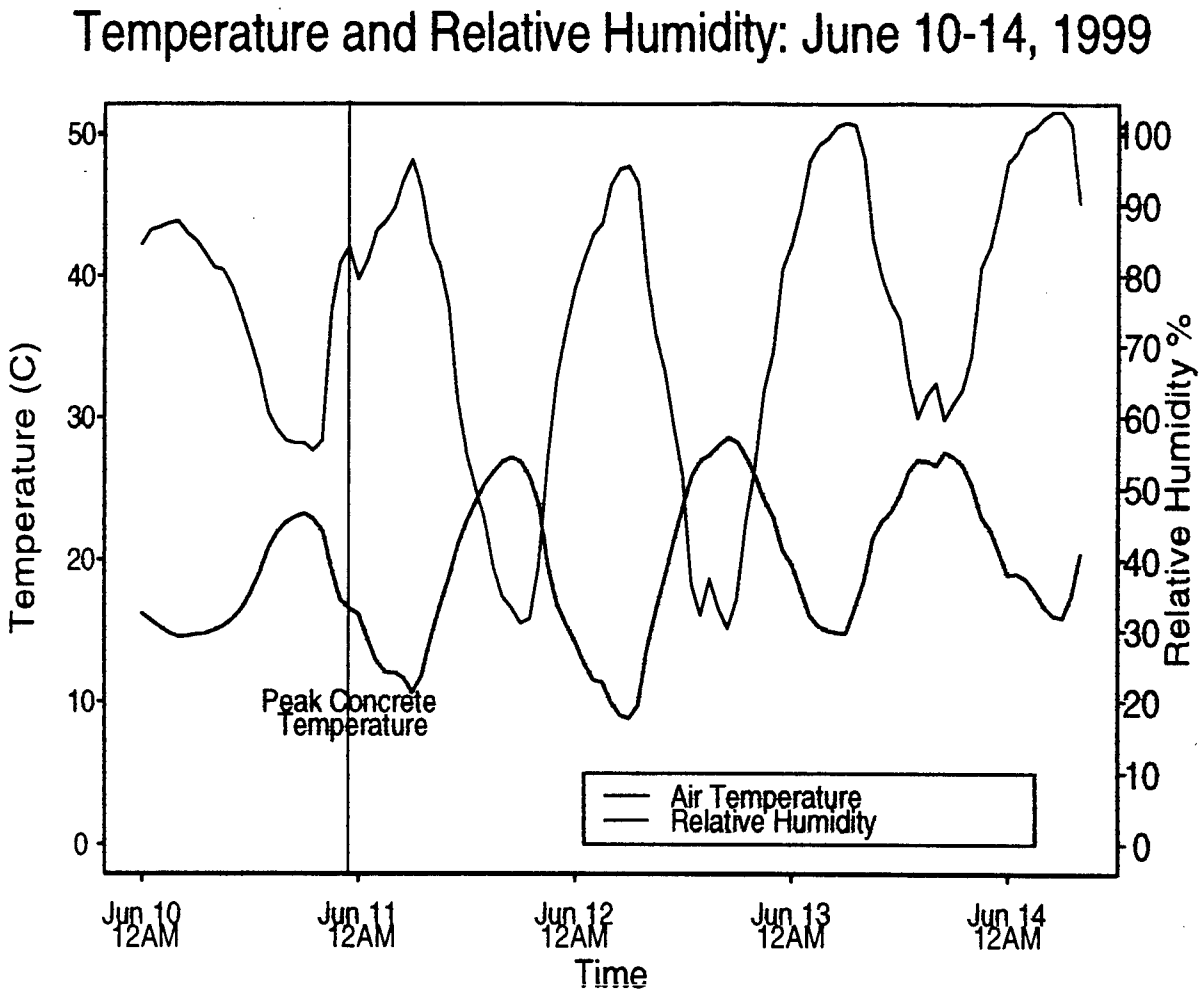

Figure 8. Hourly averaged air temperatures on the left axis and relative humidities on the right axis measured on the tower with CS500 probes.

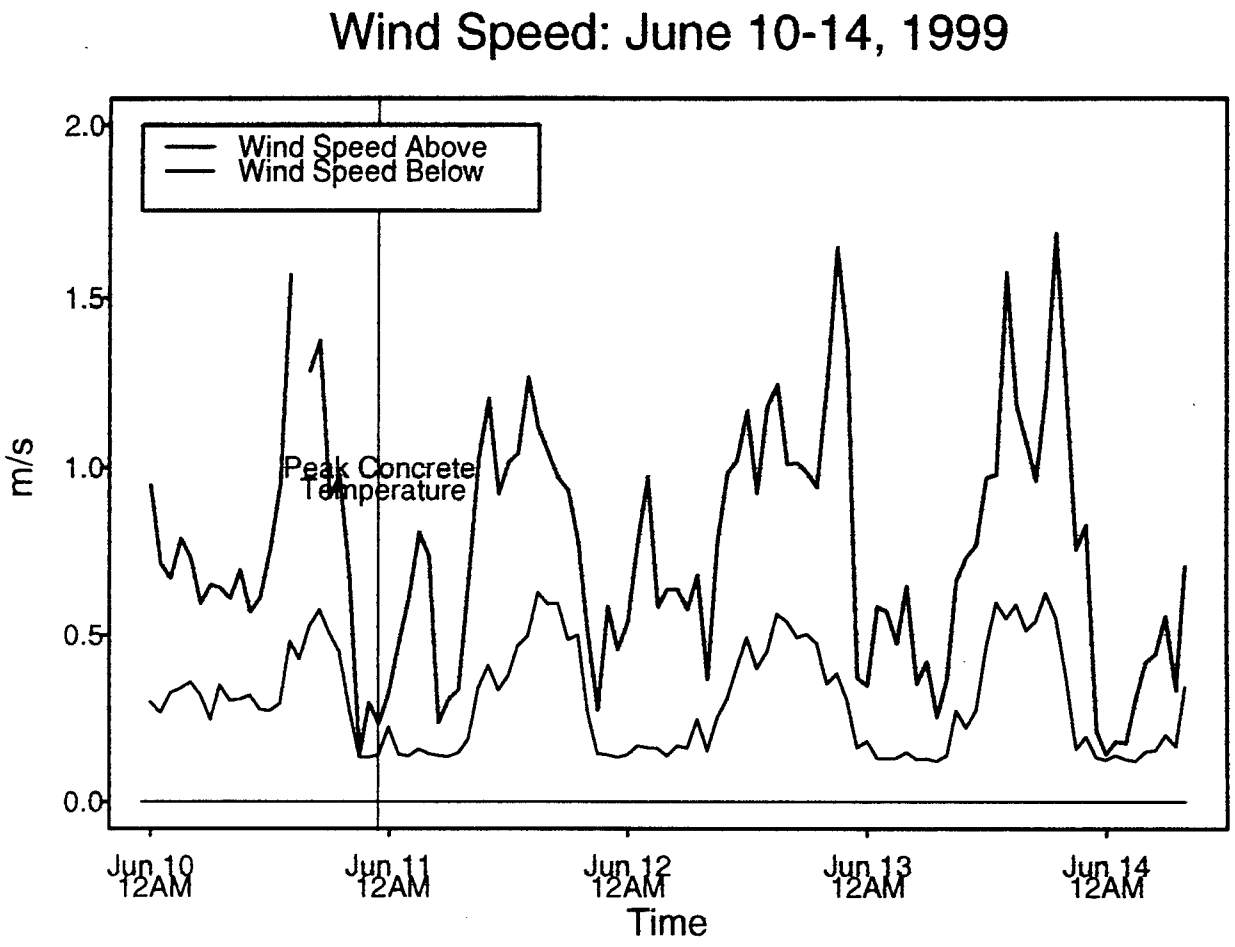

Figure 9. Wind speeds above and below the bridge deck. Wind speeds above were measured on the tower by a Gill propeller anemometer and those below by a Thornthwaite cup anemometer.

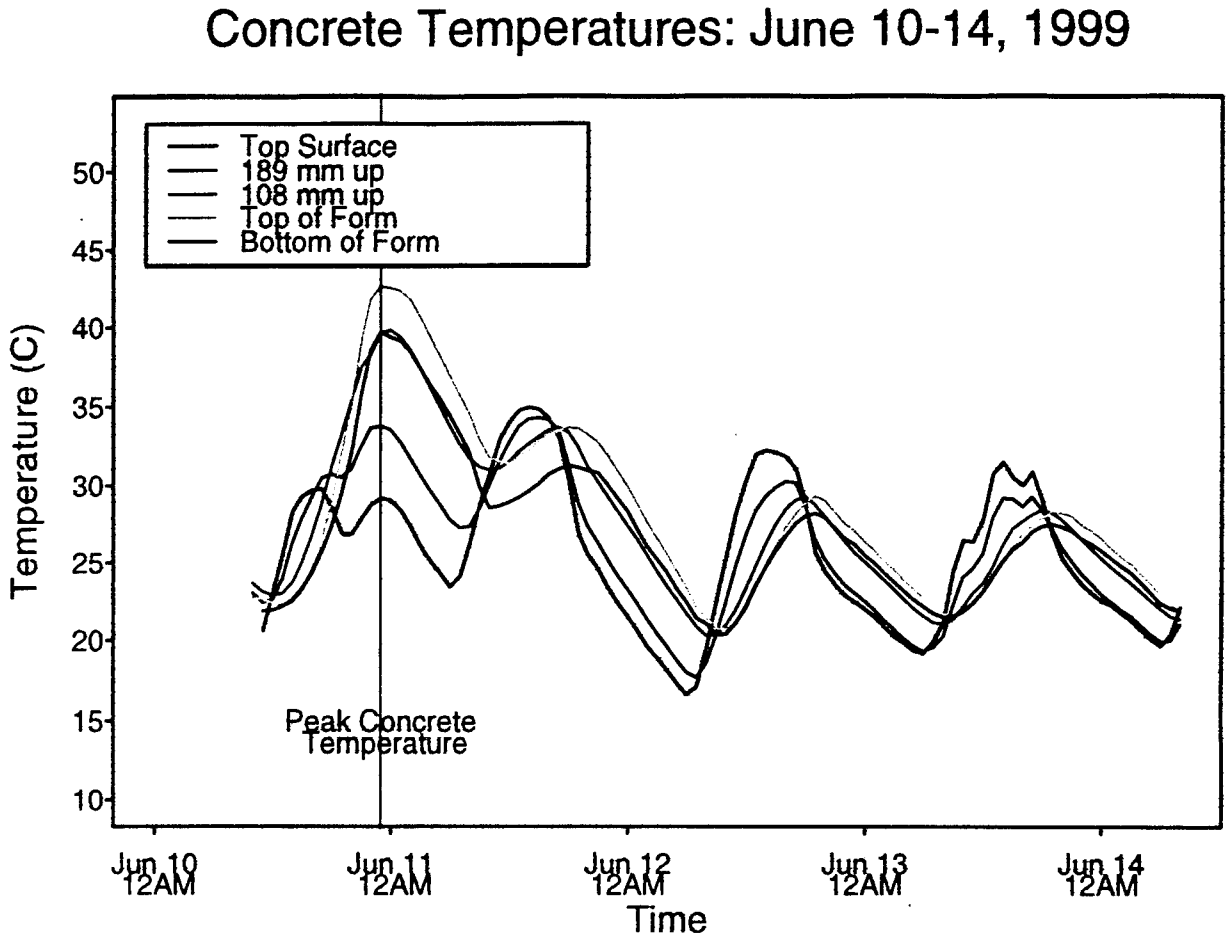

Figure 10. Hourly averaged concrete temperatures from DOT thermocouples and ASRC thermistor measurements. The DOT measurements were taken between beams 2 and 3 from the east side of the bridge. The "189 mm up" and "108 mm up" labels refer to the distance up from the top of the form where the measurements were taken.

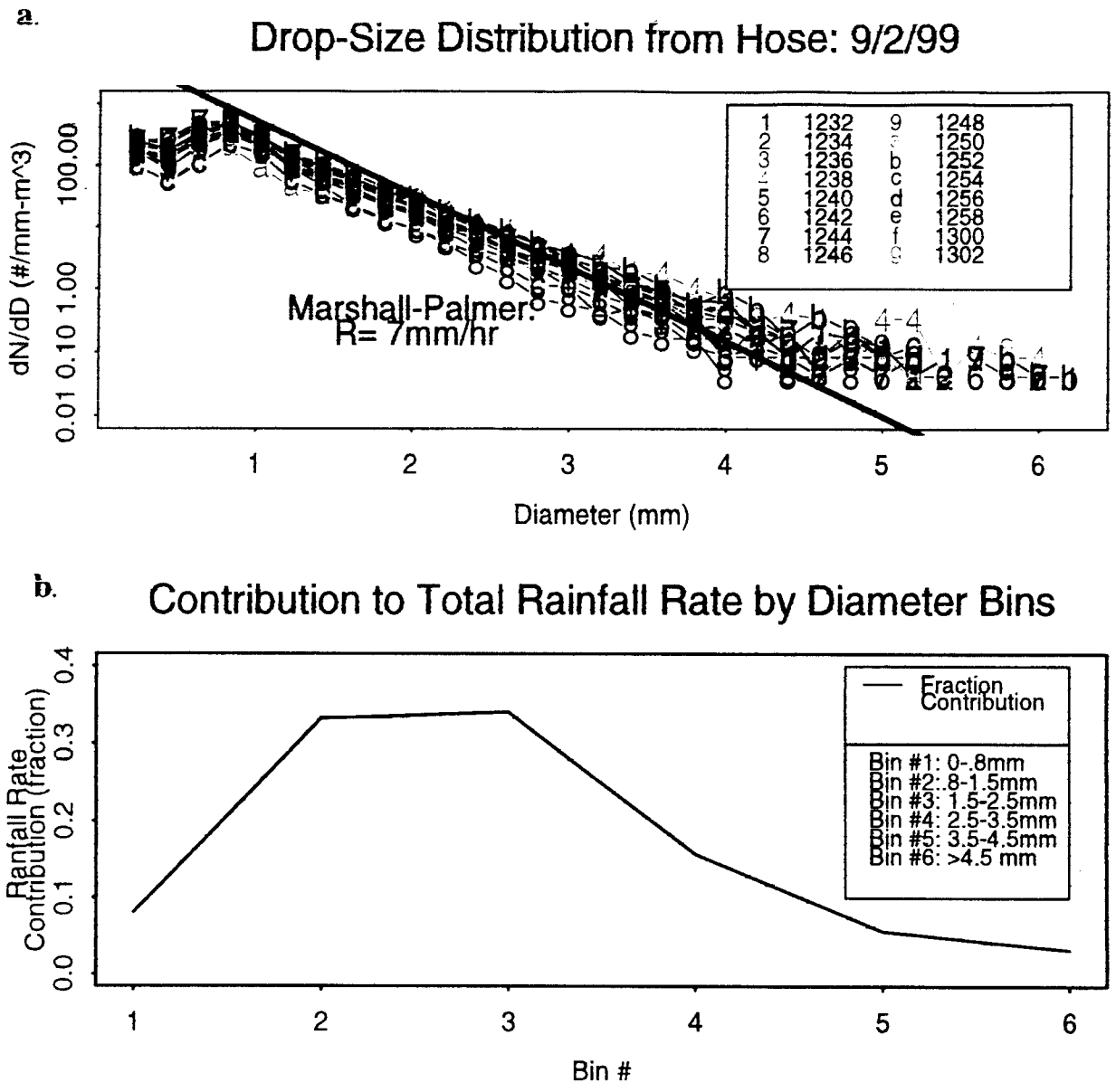

Figure 11. a. Drop size number density for water sprayed from a hose similar to that used to cure the bridge. The heavy black line is the Marshall-Palmer prediction for a rainfall rate of 7 mm/ hour. **b.** Fraction contribution to the total rainfall rate by diameter bins for the hose experiment.

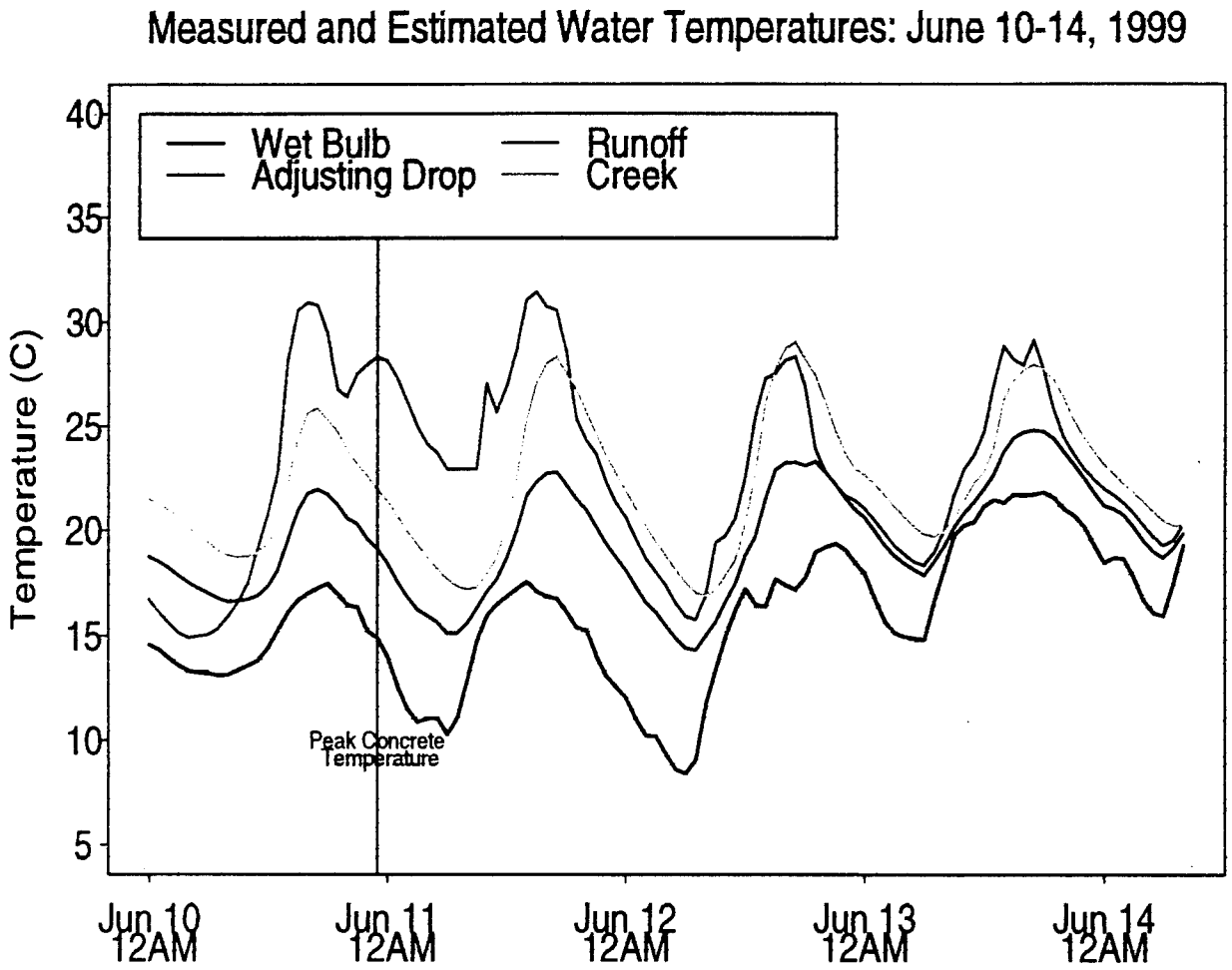

Figure 12. Measured and estimated water temperatures including the wet-bulb estimate, the estimate based on the hose experiments, and the measured creek and runoff water temperatures.

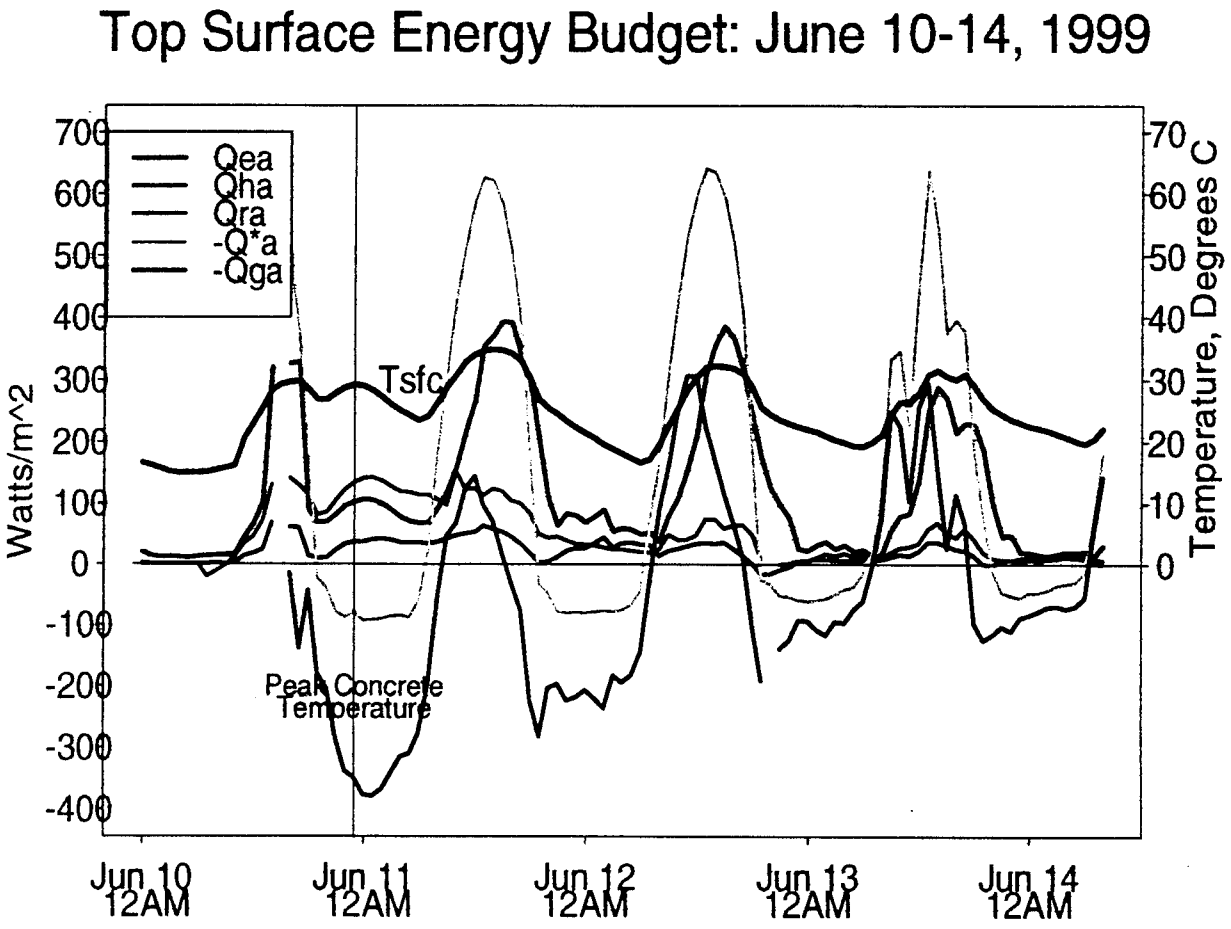

Figure 13. The top surface energy budget for Scenario 3 in which considerations are made for free convection conditions and varying surface stress by changing z_0. The red line indicates the top surface temperature from Thermistor 2.

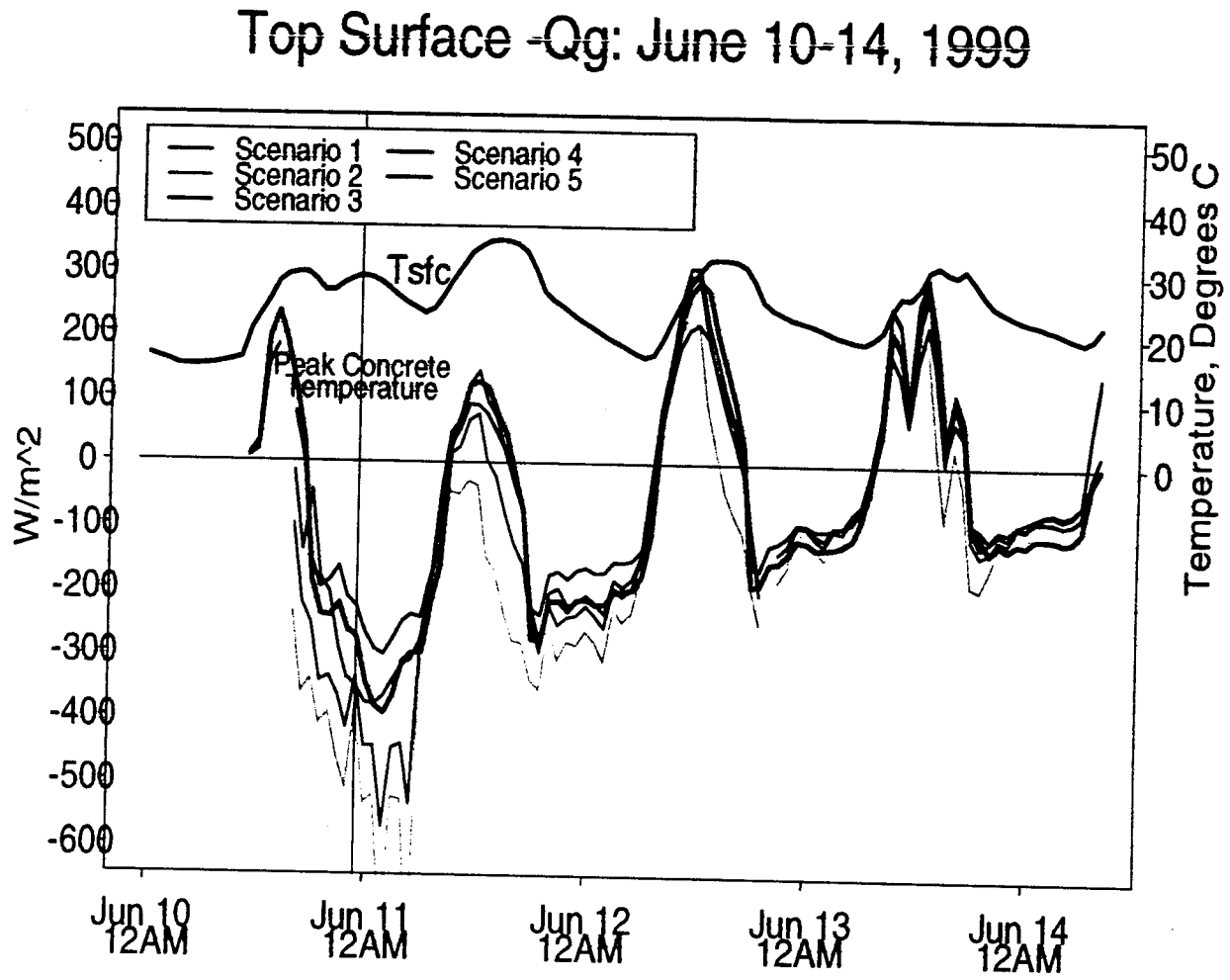

Figure 14. Various estimates of the top surface $-Q_{GA}$. Scenario 1 assumes z_0=0.005; Scenario 2 assumes z_0=0.01; Scenario 3 includes free convection and time-varying surface stress; Scenario 4 is the estimate based on the DOT thermocouple data; and Scenario 5 are values measured with the heat flux plate 1, corrected for the conductivity of the concrete. The heavy red line indicates the top surface temperature of Thermistor 2.

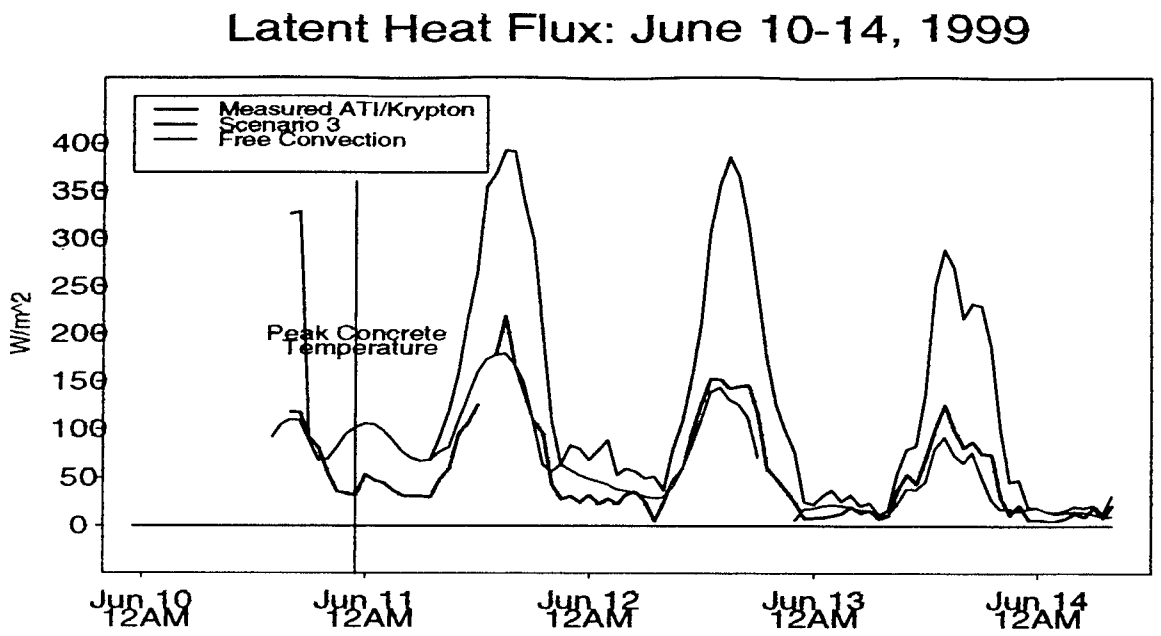

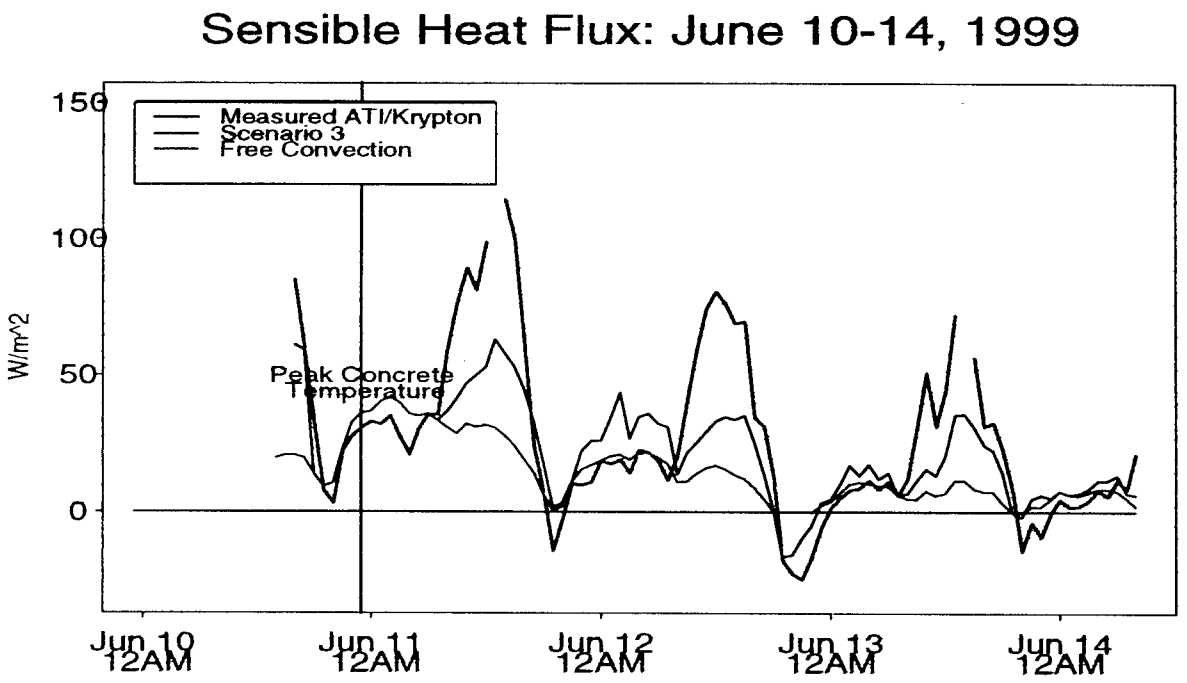

Figure 15. a. A comparison of the measured latent heat fluxes with those predicted from free convection parameterizations and from Scenario 3. **b.** As in a. but for sensible heat fluxes.

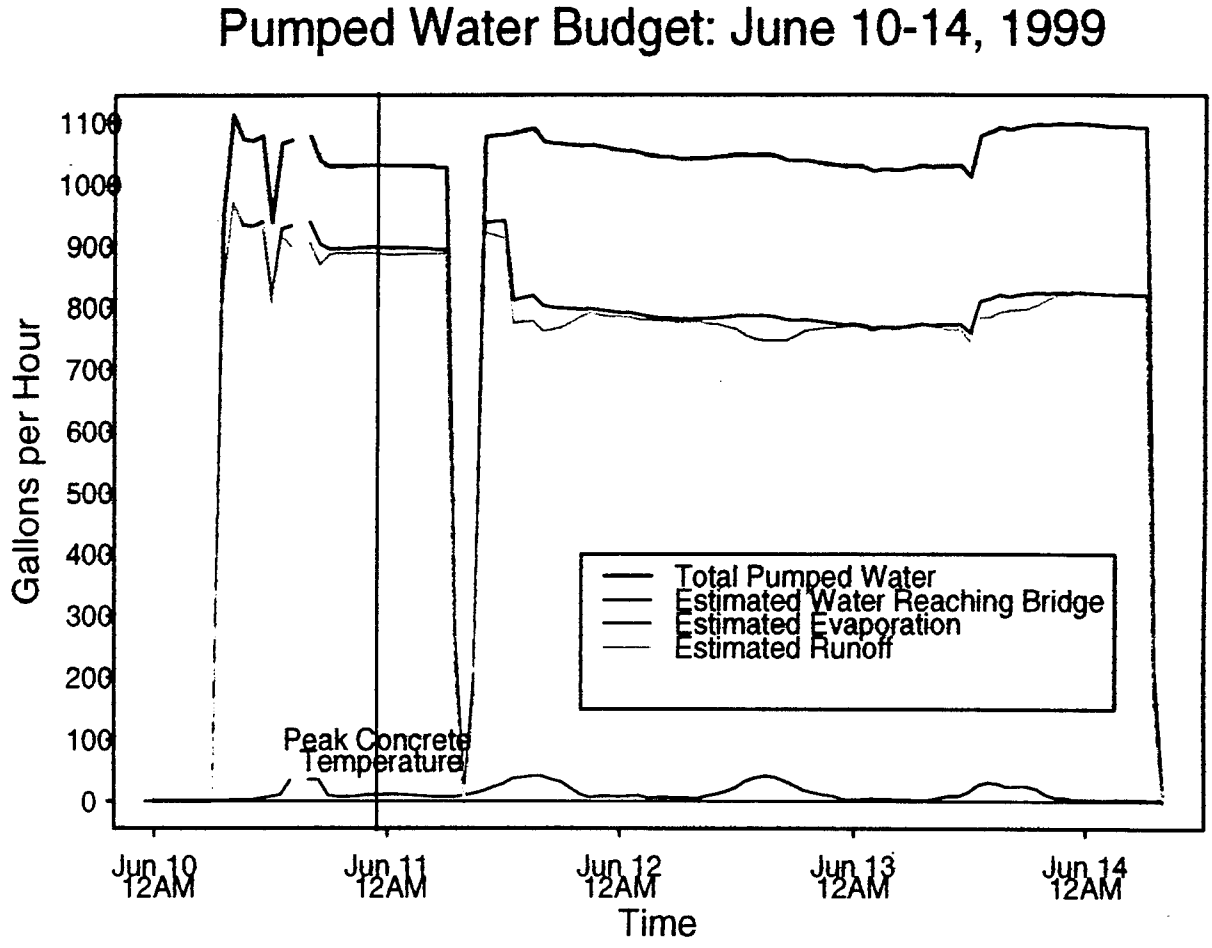

Figure 16. The budget of water pumped from the creek below the bridge. Note that not all of the "Total Pumped Water" reached the bridge as some hoses were not in contact with the bridge deck.

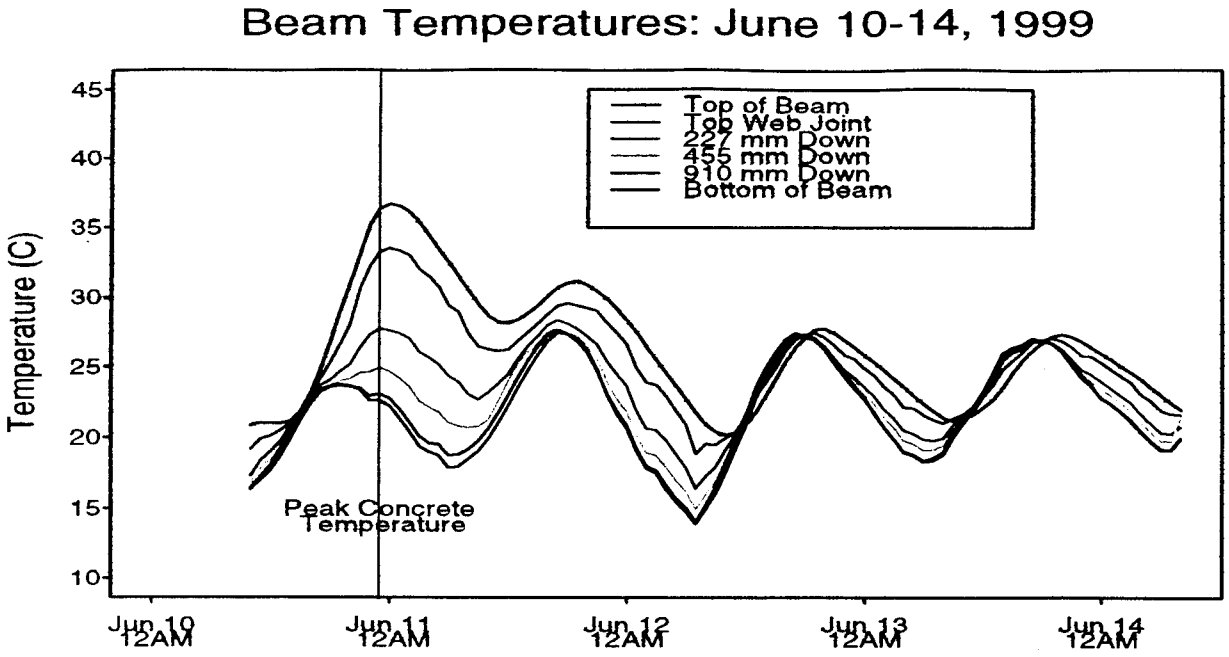

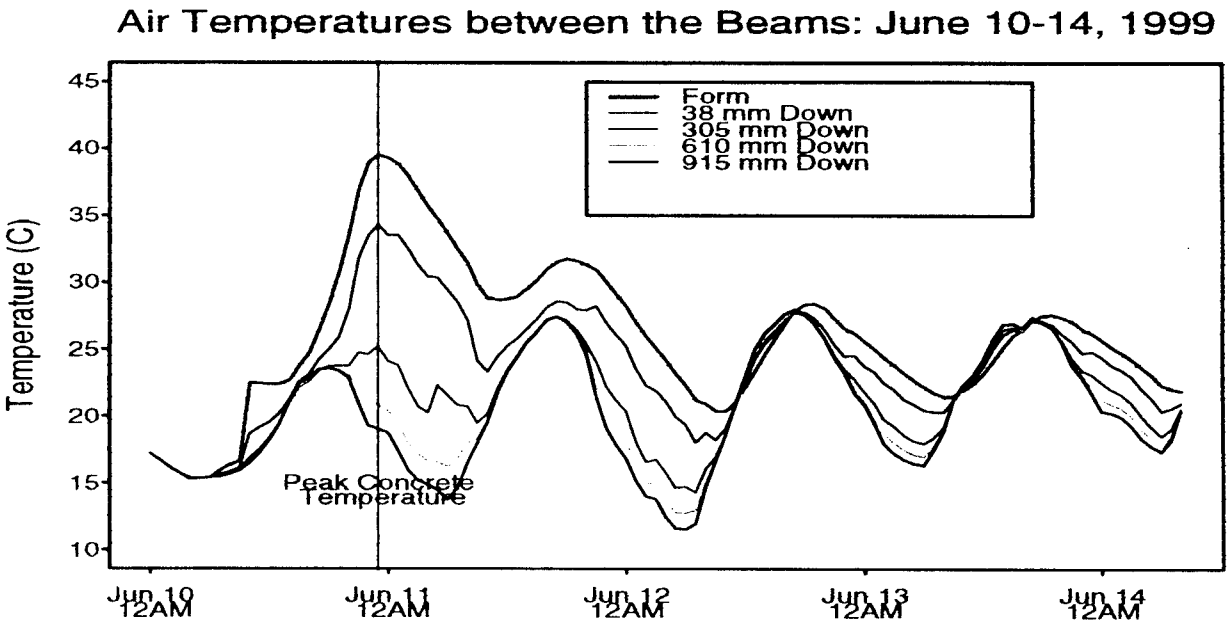

Figure 17. a. Temperatures of the center beam as measured by DOT with thermocouples. **b.** Air temperatures between the first two beams from the east as measured by ASRC thermocouples.

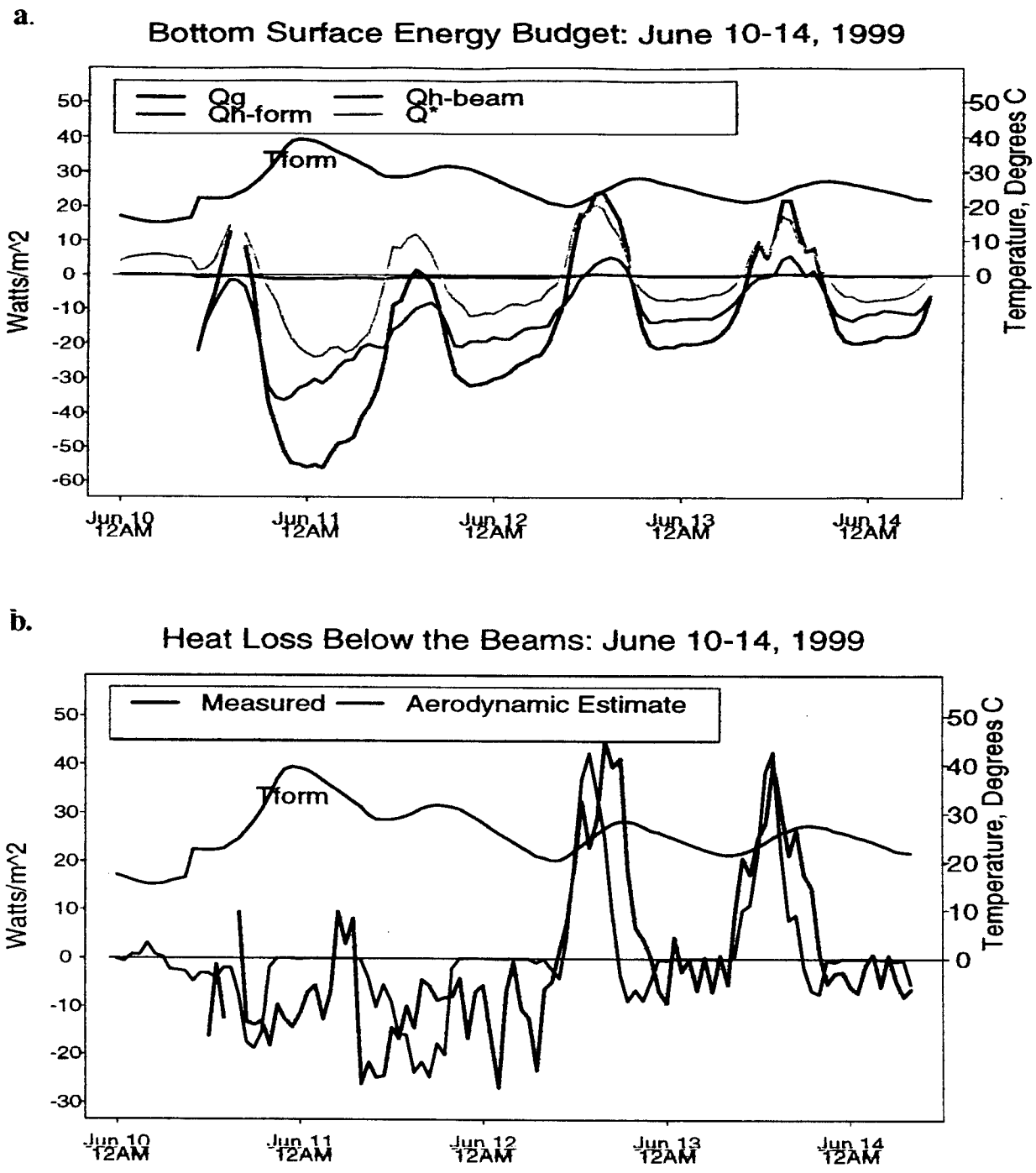

Figure 18. a. The bottom surface energy budget. The values for the components from the beam and the form have been scaled by 20% and 80%, respectively, to represent the fraction of bottom surface area they cover. **b.** The estimated and measured amount of heat removed from between the beams at the bottom of the beams.

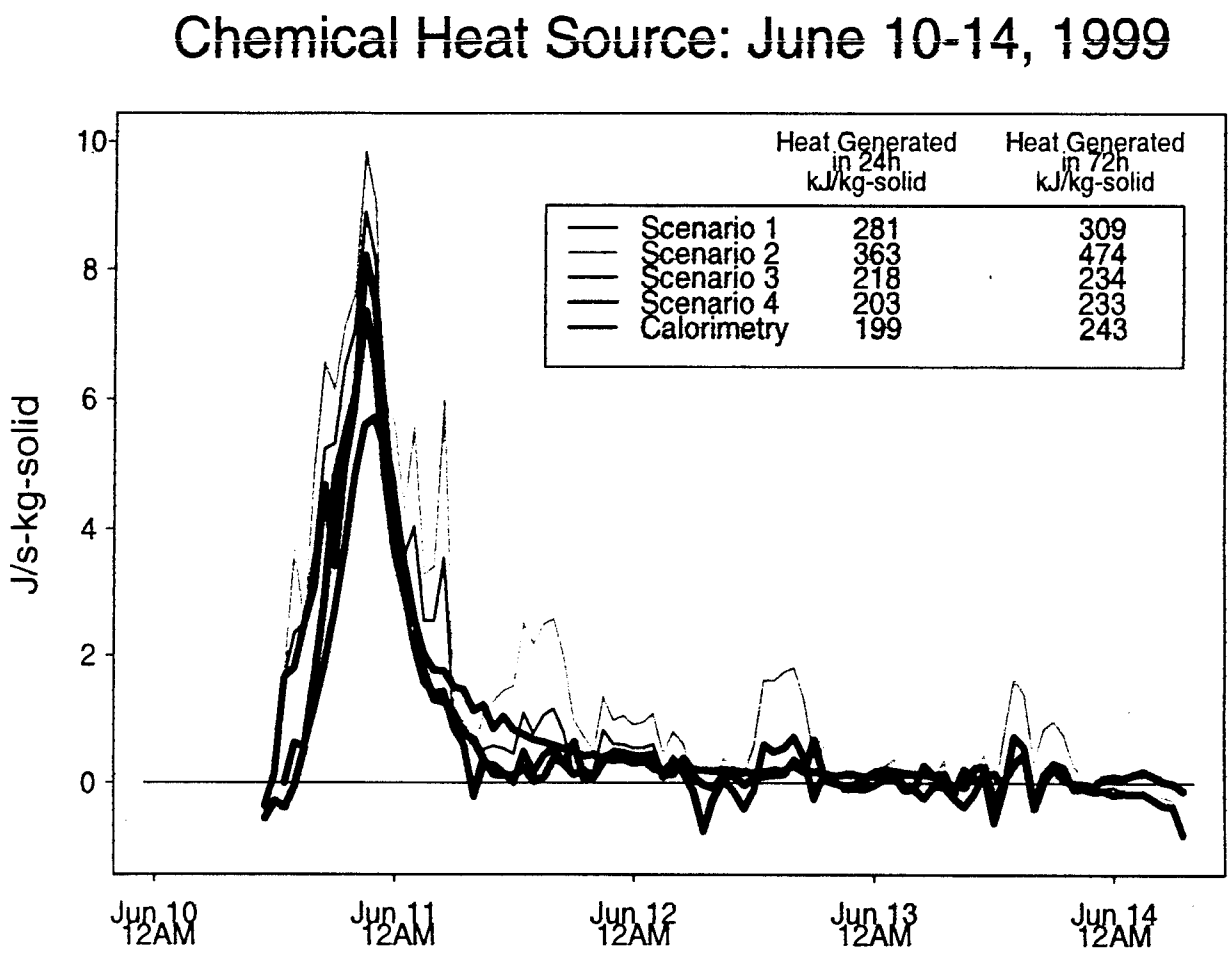

Figure 19. Estimates of the chemical heat generation rate. The Calorimetry curve was determined with the cementitious samples taken from the June 1998 bridge.